

Tight factorizations of girth- g -regular graphs

Italo J. Dejter

University of Puerto Rico
Rio Piedras, PR 00936-8377
italo.dejter@gmail.com

Abstract

Girth-regular graphs with equal girth, regular degree and chromatic index are studied for the determination of 1-factorizations with each 1-factor intersecting every girth cycle. Applications to hamiltonian decomposability and to 3-dimensional geometry are given. Applications are suggested for priority assignment and optimization problems.

1 Introduction

Let $3 \leq \kappa \in \mathbb{Z}$. Given a finite graph Γ with girth $g(\Gamma) = \kappa$, we inquire whether assigning κ colors to the edges of Γ *properly* (i.e., no two adjacent edges of same color in Γ) can be performed so that the resulting color assignment induces a bijection from the edges of Γ in each of its κ -cycles onto the κ colors. This inquiry is applicable to managerial situations in which a number of agents participate in committees about round tables, with κ seats per table. A roster of κ tasks is handed to each agent at each table, and the agent is assigned each of the κ tasks but at pairwise different tables. This can be interpreted as a 2-way (vertex incidence versus girth-cycle membership) problem of sorting the κ colors according to some prioritization hierarchies. This way, an assignment problem is conceived, with potential applications in optimization and decision making. We pass to formalize such ideas.

Let Γ be a finite connected κ -regular simple graph with chromatic index $\chi'(\Gamma) = \kappa$. Let $g = g(\Gamma)$ be the girth of Γ . We say that Γ is a *g -tight graph* if $g = g(\Gamma) = \kappa = \chi'(\Gamma)$. In each g -tight graph Γ , it makes sense to look for a proper edge-coloring via κ colors, each girth cycle colored via a bijection between the cycle edges and the colors they are assigned, precisely κ colors. We will say that such a coloring is an *edge-girth coloring* of Γ and, in such a case, that Γ is *edge-girth chromatic*, or *egc* for short.

We focus on g -tight κ -regular graphs Γ that are *girth-regular*, a concept whose definition in [17] we adapt as follows. Let Γ be one such graph. Let $\{e_1, \dots, e_\kappa\}$ be the set of edges incident in Γ to a vertex v . Let (e_i) be the number of κ -cycles containing an edge e_i , for $1 \leq i \leq \kappa$. Assume $(e_1) \geq (e_2) \geq \dots \geq (e_\kappa)$. Let the *signature* of v be the κ -tuple $((e_1), (e_2), \dots, (e_\kappa))$. The graph Γ is said to be *girth-regular* if all its vertices have a common signature. In such a case, the signature of any vertex of Γ is said to be the *signature* of Γ .

In this work, girth-regular graphs that are g -tight will be said to be *girth- g -regular graphs* as well as $((e_1), (e_2), \dots, (e_g))$ -graphs, or $(e_1)(e_2) \cdots (e_g)$ -graphs, if no confusion arises, where

$g = \kappa$. In this notation, a prefix

$$a_1^{(1)} a_1^{(2)} \cdots a_1^{(m_1)} a_2^{(1)} a_2^{(2)} \cdots a_2^{(m_2)} \cdots a_t^{(1)} a_t^{(2)} \cdots a_t^{(m_t)}$$

with $a_i^{(j)} = a_{i'}^{(j')}$ iff $i = i'$ may be abbreviated as $a_1^{m_1} a_2^{m_2} \cdots a_t^{m_t}$, where superscripts equal to 1 may be omitted (e.g., 3221 abbreviates to 32^21). So, the prefixes $(e_1)(e_2) \cdots (e_g)$ will include and further be denoted as follows:

- (i) $222 = 2^3$ and $110 = 1^20$ in Section 2, (Theorems 1 and 4);
- (ii) $3333 = 3^4$, $3322 = 3^22^2$ and $2222 = 2^4$ in Section 3, (Theorem 10, via Lemma 9);
- (iii) $4443 = 4^33$, $3221 = 32^21$ and $3111 = 31^3$ in Section 4, (Theorem 21);
- (iv) $1111 = 1^4$ in Section 5, (Theorems 24 and 27, via Lemma 9, or a variation of it);
- (v) $44400 = 4^30^2$, 2^30^2 , 8^5 and $(12)^5$ in Section 6, (Theorems 28, 29, 30 and 31).

Extending this context, girth-regular graphs Γ of regular degree g and girth larger than g will be said to be 0^g -graphs, or *improper* $(e_1)(e_2) \cdots (e_g)$ -graphs.

Edge-girth colorings of $(e_1)(e_2) \cdots (e_g)$ -graphs are equivalent to 1-factorizations [22] such that the cardinality of the intersection of each 1-factor with each girth cycle is 1. These factorizations are said to be *tight*, and the resulting colored girth cycles, are said to be *tightly colored*. Note a Γ with a tight factorization is egc. Unions of pairs of 1-factors of such graphs are treated in Section 7 for their hamiltonian decomposability, (Corollary 36). Applications to Möbius-strip compounds and hollow-triangle polylinks are found in Section 8.

2 Egcc girth-3-regular graphs

Theorem 1. [17] *There is only one $(e_1)(e_2)(e_3)$ -graph Γ with $(e_1)(e_2)(e_3) = 222 = 2^3$, namely $\Gamma = K_4$. Moreover, $\Gamma = K_4$ is egc. All other proper $(e_1)(e_2)(e_3)$ -graphs are 1^20 -graphs, but not necessarily egc.*

Proof. For the first sentence in the statement, we refer to item (1) of Theorem 5.1 [17]. To see that $\Gamma = K_4$ is egc, we refer to Fig. 1(i), below. \square

Remark 2. In order to determine which 1^20 -graphs are egc, let $\Gamma' = (V', E', \phi')$ be a finite undirected loopless cubic multigraph. Let $e \in E'$ with $\phi'(e) = \{u, v\}$ and $u, v \in V'$. Then, e determines two *arcs* (that is, ordered pairs of end-vertices of e) denoted $(e; u, v)$ and $(e; v, u)$ (if the girth $g(\Gamma')$ of Γ' is larger than 2, then Γ' is a simple graph, a particular case of multigraph). The following definition is an adaptation of a case of the definition of generalized truncation in [10]. Let A' denote the set of arcs of Γ' . A *vertex-neighborhood labeling* of Γ' is a function $\rho : A' \rightarrow \{1, 2, 3\}$ such that for each $u \in V'$ the restriction of ρ to the set $A'(u) = \{(e; u, v) \in A' : e \in E'; \phi'(e) = \{u, v\}; v \in V'\}$ of arcs leaving u is a bijection. For our purposes, we require $\rho(e; u, v) = \rho(e; v, u)$, $\forall e \in E'$ with $\phi'(e) = \{u, v\}$, so that each $e \in E'$ is assigned a well-defined color from the color set $\{1, 2, 3\}$. This yields a 1-factorization of Γ' with three 1-factors that we can call E'_1, E'_2, E'_3 for respective color 1, 2, 3, with E' being the disjoint union $E'_1 \cup E'_2 \cup E'_3$. For the sake of examples in Fig. 1, to be presented below, let colors 1, 2 and 3 be taken as red, blue and green, respectively.

Let K_3 be the triangle graph with vertex set $\{v_1, v_2, v_3\}$. The *triangle-replaced* graph $\nabla(\Gamma')$ of Γ' with respect to ρ has vertex set $\{(e_i; u, v_i) : u \in V'; 1 \leq i \leq 3\}$ and edge set

$$\{(e_i; u, v_i)(e_j; u, v_j) | v_i v_j \in E(K_3), u \in V'\} \cup \{u, v_{\rho(e; u, w)}(w, v_{\rho(e; w, u)}) | e \in E'; \phi(e) = \{u, w\}\}.$$

Note that $\nabla(\Gamma')$ is a 1^20 -graph. We will refer to the edges of the form $(e_i; u, v_i)(e_j; u, v_j)$ as ∇ -edges or *triangle edges*, and to the edges $(e_i; u, v_i)(e_j; w, v_j)$, $u \neq w$, as Γ' -edges or *non-triangle edges*. Observe that a Γ' -edge is incident only to ∇ -edges and that each vertex of $\nabla(\Gamma')$ is incident to precisely one Γ' -edge. This yields the following.

Observation 3. [10] *Let Γ' be a finite undirected cubic multigraph of girth g . Then, for any vertex-neighborhood labeling ρ of Γ' , the shortest cycle in the triangle-replaced graph $\nabla(\Gamma')$ containing a Γ' -edge is of length at least $2g$.*

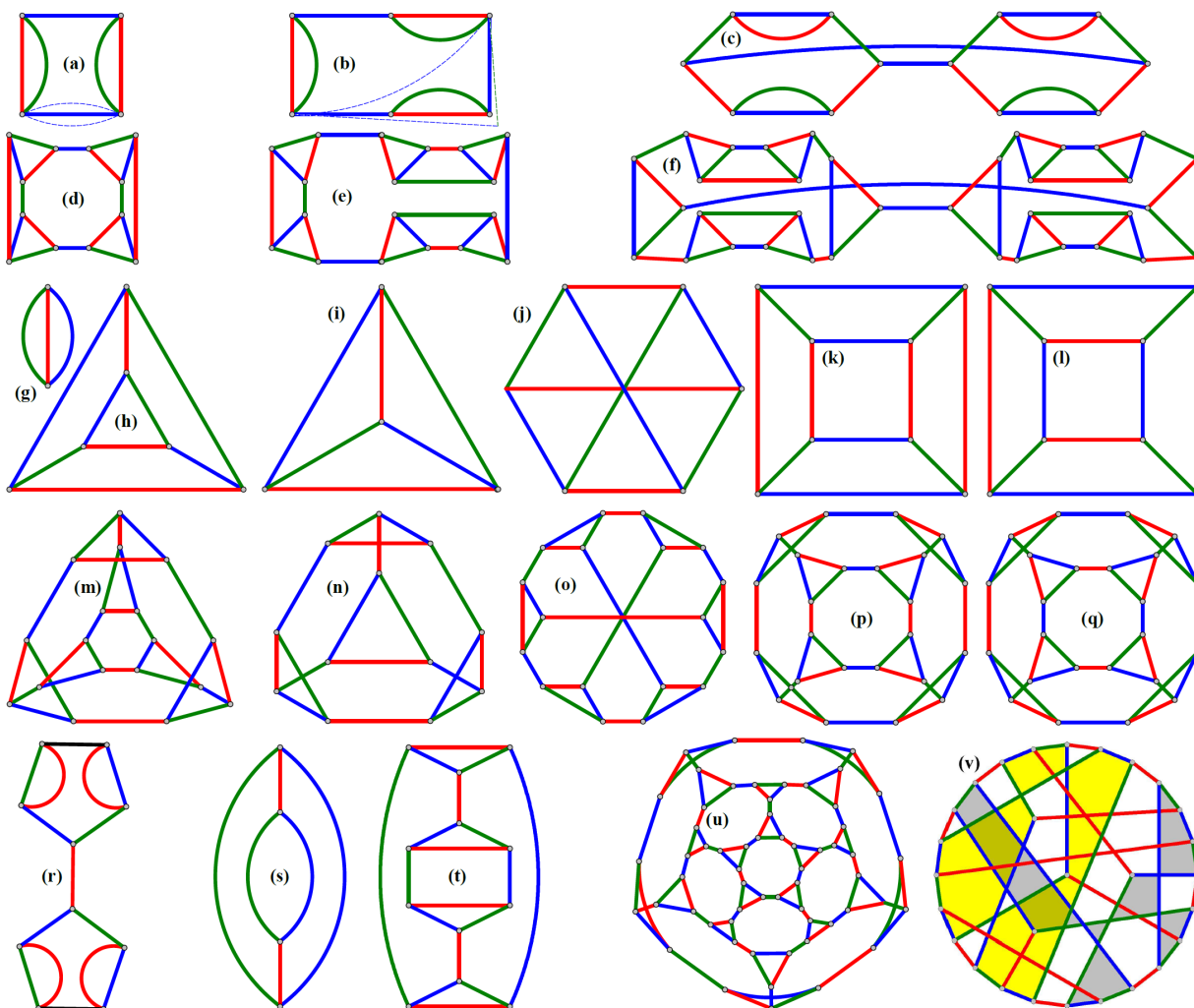


Figure 1: Producing $(e_1)(e_2)(e_3)$ -graphs that are egc.

We say that Γ' is a *generalized snark* if its chromatic index $\chi'(\Gamma')$ is larger than 3. Two examples of generalized snark are: (i) the Petersen graph and (ii) the multigraph obtained

by joining two $(2k + 1)$ -cycles ($k \geq 1$) via an extra-edge (a bridge between the two $(2k + 1)$ -cycles) and adding k parallel edges to each of the two $(2k + 1)$ -cycles so that the resulting multigraph is cubic, see Fig. 1(r) for $k = 5$. The triangle-replaced graph $\Gamma'_1 = \nabla(\Gamma')$ of a generalized snark Γ' will also be said to be a generalized snark. This denomination will also be used for the triangle-replaced graphs $\Gamma'_{i+1} = \nabla(\Gamma'_i)$ of Γ'_i , for $i = 1, 2, \dots$, etc. In addition, we will say that Γ' is *snarkless* if it is not a generalized snark. Clearly, K_4 is snarkless.

Vertex-neighborhood labelings ρ for the examples of Γ' below, represented in Fig. 1, have the elements 1, 2 and 3 of $\rho(A')$ interpreted respectively as edge colors red, blue and green. Now, the smallest snarkless multigraphs $\Gamma' \neq K_4$ are:

- (A) the cubic multigraph Γ'_A of two vertices and three edges in Fig. 1(g), with $\nabla(\Gamma'_A)$ being the triangular prism $\text{Prism}(K_3) = K_2 \square K_3$, in Fig. 1(h), where $V(K_2) = \{0, 1\}$ and \square stands for the graph cartesian product [15];
- (B) the cubic multigraph Γ'_B of four vertices resulting as the edge-disjoint union of a 4-cycle and a 2-factor $2K_2$ in Fig. 1(a), with $\nabla(\Gamma'_B)$ in Fig. 1(d).

Given a snarkless Γ' , a new snarkless multigraph Γ'' is obtained from Γ' by replacing any edge e with end-vertices say u, v , by the submultigraph resulting as the union of a path $P_4 = (u, u', v', v)$ and an extra edge with end-vertices u', v' . For example, Γ' in Fig. 1(g) as Γ'' in Fig. 1(s) and $\nabla(\Gamma'')$ in Fig. 1(t). Using this replacement of an edge e by the said submultigraph, one can transform the submultigraph Γ'_B with the enclosed blue edge e in item (B), above, into a Γ''_B as in Fig. 1(b), with $\nabla(\Gamma''_B)$ in Fig. 1(e); or with the four red and green edges into a Γ''_B as in Fig. 1(c), with $\nabla(\Gamma''_B)$ in Fig. 1(f).

The triangle-replaced graph $\nabla(\Gamma')$ of any snarkless $(e_1)(e_2)(e_3)$ -graph Γ' , either proper or improper, with $(e_1)(e_2)(e_3) \in \{2^3, 1^20, 0^3\}$, yields an egc 1^20 -graph, illustrated via the four graphs in Fig. 1(h–k), namely $\Gamma' = \nabla(\Gamma'_A)$, K_4 , $K_{3,3}$ and Q_3 (the 3-cube graph), onto the four 1^20 -graphs Γ in Fig. 1(m–p). This raises the observation that non-equivalent 1-factorizations F, F' of an $(e_1)(e_2)(e_3)$ -graph Γ' , like in Fig. 1(k–l) for $\Gamma' = Q_3$, result in non-equivalent 1-factorizations $\nabla(F), \nabla(F')$ of $\Gamma = \nabla(\Gamma')$, represented in this case on $\Gamma = \nabla(\Gamma') = \nabla(Q_3)$ in Fig. 1(p–q). This leads to the final assertion in Theorem 4, below.

Fig. 1(u) is the egc 1^20 -graph given by $\nabla(\Gamma')$ for the dodecahedral graph $\text{Dod} = \Gamma'$, in which the union of any two edge-disjoint 1-factors of a 1-factorization of Γ' yields a Hamilton cycle. In contrast, the Coxeter graph $\text{Cox} = \Gamma'$ in Fig. 1(v) is non-hamiltonian, but the union of any two of its (edge-disjoint) 1-factors is the disjoint union of two 14-cycles, whose apparent interiors are shaded yellow and light gray in the figure. Thus, $\Gamma = \nabla(\Gamma')$ is an egc 1^20 -graph.

Theorem 4. *A 1^20 -graph Γ is egc if and only if Γ is the triangle-replaced graph of a snarkless Γ' . Moreover, non-equivalent 1-factorizations of such Γ' result in corresponding non-equivalent 1-factorizations of Γ .*

Proof. There are two types of edges in a 1^20 -graph Γ , namely the *triangle edges* (those belonging to some triangle of Γ) and the remaining *non-triangle edges*. Each vertex v of Γ is incident to a unique non-triangle edge e_v and is nonadjacent to a unique edge \bar{e}_v (opposite to v) in the sole triangle T_v of Γ to which v belongs. In any 1-factorization $F = (F_1, \dots, F_g)$ of

Γ , both e_v and \bar{e}_v belong to the same factor F_i ($i = 1, \dots, g$). Moreover, each edge $e = \{u, v\}$ of Γ (where $e = e_u = e_v$) belongs solely to corresponding triangles T_u and T_v with opposite edges \bar{e}_u and \bar{e}_v . Clearly, $\{e = e_u = e_v, \bar{e}_u, \bar{e}_v\} \subseteq F_i$ with equality given precisely when Γ is the triangular prism in Fig. 1(h).

We will define an inverse operator ∇^{-1} of ∇ that applies to each egc 1²0-graph Γ . Given one such Γ , contracting simultaneously all the triangles T of Γ consists in removing the edges of those T and then identifying the vertices v_1^T, v_2^T, v_3^T of each T into a corresponding single vertex v_T , where v_i^T , for $i \in \{1, 2, 3\}$, has its unique incident non-triangle edge of Γ with color i . This is done so that whenever two triangles T and T' have respective vertices v_i^T and $v_j^{T'}$ adjacent in Γ ($i, j \in \{1, 2, 3\}$), then $i = j$ and the edge $v_i^T v_j^{T'}$ of Γ is removed and replaced by a new edge $v_T v_{T'}$. The result of these simultaneous triangle contractions is a multigraph $\Gamma' = (V', E', \phi')$ with each $v_T \in V'$ incident to three edges of E' , one per each color in $\{1, 2, 3\}$. The ensuing edge coloring in Γ' corresponds to a vertex-neighborhood labeling $\rho : A' \rightarrow \{1, 2, 3\}$ of Γ' , from which it follows that Γ is the triangle-replaced graph of Γ' with respect to ρ , that is: $\nabla^{-1}(\Gamma) = \Gamma'$. This establishes an identification of Γ and $\nabla(\Gamma')$ so that the triangle-edges of Γ are the ∇ -edges of $\nabla(\Gamma')$, and the non-triangle edges Γ are the Γ' -edges of $\nabla(\Gamma')$. This implies the main assertion of the statement of the theorem. \square

3 Egc girth-4-regular graphs

Remark 5. In this section and in Section 4, we consider $(e_1)(e_2)(e_3)(e_4)$ -graphs Γ with $(e_1)(e_2)(e_3)(e_4) \neq 1111$. Many such graphs are toroidal and obtained from the square tessellation denoted by its Schläfli symbol $\{4, 4\}$. Let T be the group of translations of the plane that preserve such tessellation $\{4, 4\}$. Then, T is isomorphic to $\mathbb{Z} \times \mathbb{Z}$ and acts transitively on the vertices of $\{4, 4\}$. If U is a subgroup of finite index in T , then $\mathcal{M} = \{4, 4\}/U$ is a finite map of type $\{4, 4\}$ on the torus, and every such map arises this way ([24], Section 6). A symmetry α of $\{4, 4\}$ acts as a symmetry of \mathcal{M} if and only if α normalizes U . Every such \mathcal{M} has symmetry group $\text{Aut}(\mathcal{M})$ transitive on vertices, horizontal edges and vertical edges. Moreover, for each edge e of \mathcal{M} , there is a symmetry that reverses e . The tessellation $\{4, 4\}$ may be considered as a lattice, so it has a *fundamental region* [4, 5]. Such region will be called a *cutout* Φ and be given by a rectangle r squares wide and t squares high, with the left and right edges identified by parallel translation in order to get a toroidal embedding of Γ , and the bottom edges identified with the top edges after a shift of s squares to the right, as in Fig. 6 of [24]. A toroidal graph with such a cutout will be denoted $\{4, 4\}_{r,t}^s$. While the aim of [18, 19, 24] is the study of edge-transitive graphs, we find 1-factorizations of g -tight graphs in graphs $\{4, 4\}_{r,t}^s$ of a more ample nature. Our notation for the vertices of those cutouts will be (i, j) , or ij if no confusion arises, where $0 \leq i < r$ and $0 \leq j < t$, as in the examples of tight factorizations in Fig. 2(d–j). For $t > 1$ as in Fig. 2(d–g), the notation arises from the fact that $\{4, 4\}$ can be considered as the undirected Cayley graph of the direct-sum group $\mathbb{Z} \oplus \mathbb{Z}$ with generator set formed by $(1, 0)$ for horizontal left-to-right arcs and $(0, 1)$ for vertical up-to-down arcs. In case $t = 1$ (Fig. 2(c, h–j)), we simplify notation by writing i , instead of $(i, 0)$ or $i0$. In Fig. 2, edge colors are encoded by numbers as follows: 1 for red, 2 for blue, 3 for green and 4 for hazel. (Thin and dashed diagonals of squares are to be used in the proof of Theorem 10).

Remark 6. If a fundamental region Φ of $\{4, 4\}$ as in Remark 5 is identified in reverse on a pair \mathcal{P} of opposite sides, and directly on the other pair, we get a Klein bottle \mathcal{K} [23]. There are egc-graphs that are skeletons of a $\{4, 4\}$ -tessellation of \mathcal{K} , for example in Fig. 2(b), whose embedding into \mathcal{K} has corresponding cutout that can be obtained from the one of $\{4, 4\}_{r,t}^s$ above (with $(r, t, s) = (6, 3, 0)$) first by replacing the vertical edges by corresponding square-face diagonals, while keeping the horizontal edges (so the new faces are lozenge rhombi), and second by identifying the horizontal top and bottom borders of the original cutouts, as well as the left and right borders, these with reverse orientations, with the resulting \mathcal{K} -embedding that we will denote $[4, 4]_{r,t}^s$. Then, the example of Fig. 2(b) is in $[4, 4]_{6,3}^0$. If Φ is identified in reverse on both pairs of opposite sides, a projective-planar graph is obtained. This can be ruled out because $\{4, 4\}$ -tessellations only exist on surfaces with Euler characteristic 0.

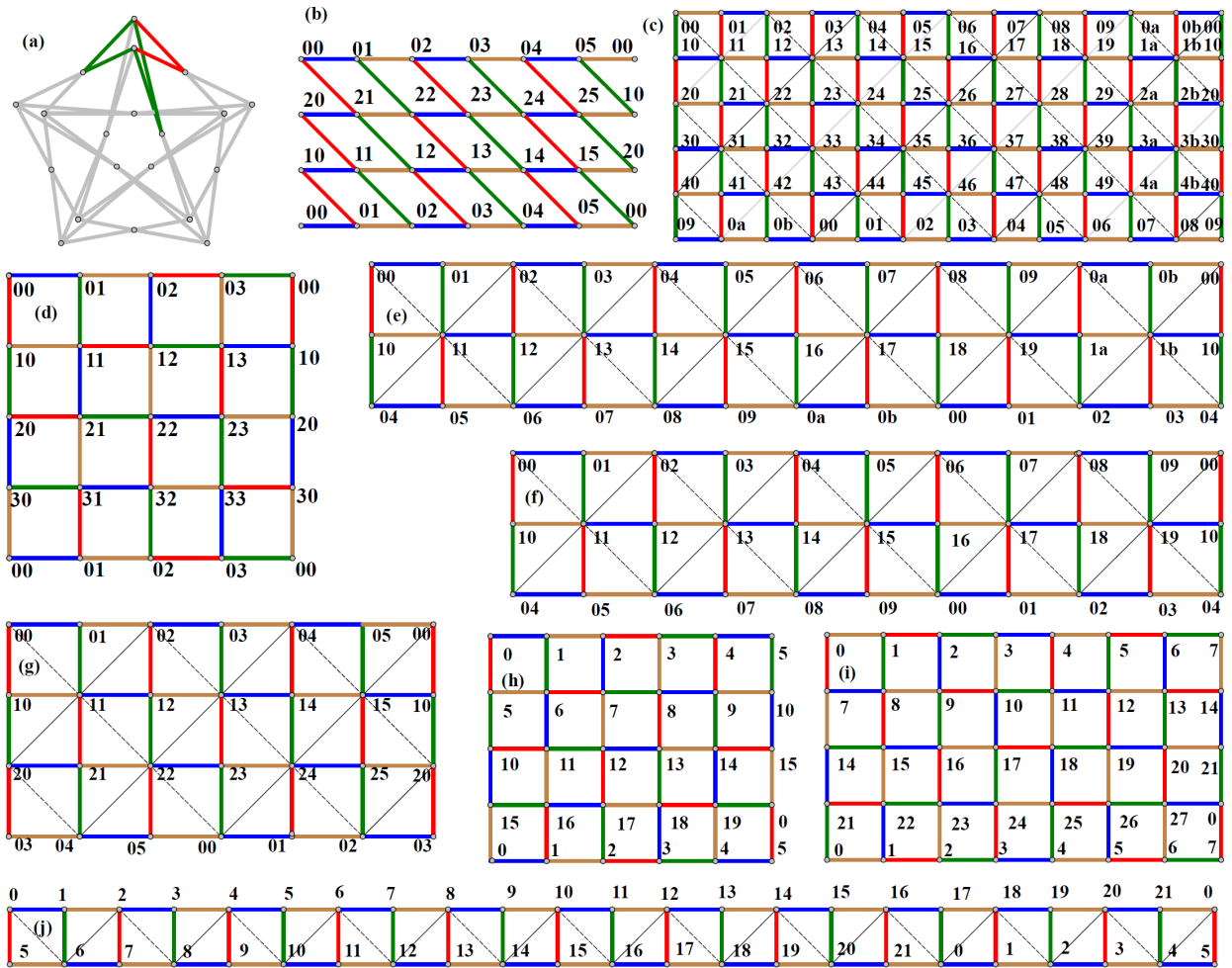


Figure 2: Examples of $(e_1)(e_2)(e_3)(e_4)$ -graphs.

Remark 7. Let $0 < n \in \mathbb{Z}$. The n -cube graph Q_n has as vertices the n -tuples with entries in \mathbb{Z}_2 and edges only between vertices at unit Hamming distance. In Subsection 3.1, we consider the 4-cube graph $Q_4 = \{4, 4\}_{4,4}^0$. Other $(e_1)(e_2)(e_3)(e_4)$ -graphs with $(e_1)(e_2)(e_3)(e_4) \neq 1111$ and that are not prisms of $(e_1)(e_2)(e_3)$ -graphs are:

- (i) the bipartite complement of the Heawood graph, in Subsection 3.3;
- (ii) the *subdivided double* $\mathbb{D}\Gamma$ [18, 24] of a 4-regular graph Γ is the bipartite graph with vertex set $(V(\Gamma) \times \mathbb{Z}^2) \cup E(\Gamma)$ and an edge between vertices $(v, i) \in V(\Gamma) \times \mathbb{Z}^2$ and $e \in E(\Gamma)$ whenever v is incident to e in Γ ; [18, Lemma 4.2] asserts that if Γ is 4-regular and arc-transitive, then $\mathbb{D}\Gamma$ is 4-regular and semisymmetric; for example, the Folkman graph (Fig. 2(a)) is the subdivided double $\mathbb{D}K_5$ of the complete graph K_5 ;
- (iii) the *circulant graphs*, i.e. the Cayley graphs $C_n(i, j)$ of the cyclic group \mathbb{Z}_n ($n > 6$) with generating sets $\{\pm i, \pm j\}$, where $1 \leq i < j < \frac{n}{2}$, and $\gcd(n, i, j) = 1$; most of these are 2^4 -graphs (assuming n even, otherwise chromatic index is not 4), with additional cycles appearing whenever a congruence $\lambda i \pm (4 - \lambda)j \equiv 0 \pmod{n}$ holds, (e.g., $C_{14}(2, 3)$ is a 2^4 -graph, $C_{12}(2, 3)$ is a $3^2 2^2$ -graph, $C_{10}(1, 3)$ is a 6^4 -graph and $C_8(1, 3) \equiv K_{4,4}$ is a 9^4 -graph); however, such graphs $C_n(i, j)$ can always be seen as toroidal graphs;
- (iv) the *wreath graphs* $W(n, 2) = C_n[\overline{K_2}]$ ($n > 4$), i.e. lexicographic products of an n -cycle and the complement $\overline{K_2}$ of K_2 ; these are 5^4 -graphs; ($W(4, 2) \equiv K_{4,4}$ is a 9^4 -graph).

Remark 8. If an $(e_1)(e_2)(e_3)(e_4)$ -graph Γ as in Remark 7 contains a subgraph Γ' guaranteeing that Γ is not an egc-graph, then Γ' is said to be an *egc-obstruction*. A subgraph $\Gamma' \equiv K_{2,3}$ is an egc-obstruction for a girth-4-regular graph Γ , since each of the proper edge-colorings of Γ contains a quadrangle of Γ' with only two colors. In Fig. 2(a), one such graph Γ , namely the Folkman graph $\Gamma = \mathbb{D}K_5$ is presented with a subgraph $\Gamma' \equiv K_{2,3}$ formed by a green quadrangle and a red 2-path. $C_{10}(1, 3)$ and $W(6, 2)$ also have obstruction isomorphic to $K_{2,3}$.

The following lemma is a tool for Theorems 9 and 27, and a variation of it, for Theorem 24.

Lemma 9. *A sufficient condition for an $(e_1)(e_2)(e_3)(e_4)$ -graph Γ with $(e_i) < 3$ ($i = 1, 2, 3, 4$) to be egc is existence of 2-factorization $\{F_1, F_2\}$ of Γ such that each 2-factor F_i ($i = 1, 2$):*

1. *is the disjoint union of even-length cycles; and*
2. *has an even-length cycle $D(C)$ as in item 1, for each 4-cycle C of Γ , sharing with C exactly two consecutive edges.*

Proof. A 1-factorization of F_1 via colors 1 and 2 and a 1-factorization of F_2 via colors 3 and 4 exist and form a tight 1-factorization of Γ . □

Theorem 10. *The following 3^4 -, $3^2 2^2$ - and 2^4 -graphs exist, and are egc or not, as indicated:*

1. *3^4 -graphs comprising the:*
 - (a) *bipartite complement of the Heawood graph, which is not egc, (Subsection 3.3);*
 - (b) *4-regular subdivided doubles $\mathbb{D}\Gamma$ of 4-regular graphs Γ , which are not egc;*
 - (c) *4-cube graph $Q_4 = \{4, 4\}_{4,4}^0$, which is egc in two different, orthogonally related ways, (Subsections 3.1-3.2, Remark 11; an initial example is in Fig. 2(d));*

2. 2^23^2 -graphs (assuming $0 < t \leq r$ and $0 \leq s < r$), comprising:

- (a) $\{4, 4\}_{2\ell, 4}^0$: $\text{egc} \Leftrightarrow \ell \in (3, \infty) \cap 2\mathbb{Z}$; (concatenating copies of $\{4, 4\}_{4, 4}^0$, in Fig. 2(d));
- (b) $\{4, 4\}_{4s, 1}^s$: $\text{egc} \Leftrightarrow s \in (4, \infty) \cap \mathbb{Z} \setminus 2\mathbb{Z}$; (Fig. 2(h-i), for $r_t^s = 20_1^5, 28_1^7$);

3. 2^4 -graphs (assuming $0 < t \leq r$ and $0 \leq s < r$) comprising:

- (a) $\{4, 4\}_{r, 1}^s$: $\text{egc} \Leftrightarrow r \in 2\mathbb{Z} \setminus 4\mathbb{Z}$, $s \in \mathbb{Z} \setminus (2\mathbb{Z} \cup 1)$ and $r \neq 3s + 1$; (Fig. 2(j), $r_t^s = 22_1^5$);
- (b) $\{4, 4\}_{r, 2}^s$: $\text{egc} \Leftrightarrow r \in [10, \infty) \cap 2\mathbb{Z}$ and $s \in [4, r-4] \cap 2\mathbb{Z}$; (Fig. 2(e-f), $r_t^s = 12_2^4, 10_2^4$);
- (c) $\{4, 4\}_{r, 3}^s$: $\text{egc} \Leftrightarrow r \in [6, \infty) \cap 2\mathbb{Z}$ and $s = [3, r-3] \setminus 2\mathbb{Z}$; (Fig. 2(g), $r_t^s = 6_3^3$);
- (d) $\{4, 4\}_{r, 4}^s$: $\text{egc} \Leftrightarrow 4 \leq r \in 2\mathbb{Z}$ and $0 < s \in 2\mathbb{Z}$; (color pattern as in Fig. 2(e-g), (j));
- (e) $\{4, 4\}_{r, t}^s$, $t \in [4, \infty)$: $\text{egc} \Leftrightarrow r \in 2\mathbb{Z}$ and $t + s \in 2\mathbb{Z}$; (color pattern as in Fig. 2(c));
- (f) $[4, 4]_{r, t}^0$: $\text{egc} \Leftrightarrow r \in [6, \infty) \cap 2\mathbb{Z}$ and $t \in [3, \infty) \cap \mathbb{Z} \setminus 2\mathbb{Z}$; (Fig. 2(b), $r_t^s = 6_3^0, 8_3^0$).

A cycle of a graph Γ as in Remarks 5-6 is said to be *1-zigzagging* if it is formed by alternate horizontal and non-horizontal (i.e., all vertical or all 45° -tilted) edges. A 2-factor of Γ is said to be *1-zigzagging* if its composing cycles are 1-zigzagging. A 2-factorization of Γ is said to be *1-zigzagging* if its composing 2-factors are 1-zigzagging.

Proof. We pass to analyze the different items composing the statement of Theorem 10.

Items 1 and 2: Item 1(a) is proved in Subsection 3.3. The graphs of item 1(b) have egc-obstructions (see Remark 8) formed by three edge-disjoint paths of length 2 between two nonadjacent vertices, e.g., $\mathbb{D}K_5$ in Fig. 2(a), with egc-obstruction formed by four green edges and two red edges. Items 1(c) and 2(b) are proved in Subsection 3.2, Remark 11; (see also Fig. 2(d)). Item 2(a) is proved by concatenating copies of $\{4, 4\}_{4, 4}^0$, as in Fig. 2(d).

Item 3: Lemma 9 applies to each Γ as in Remarks 5-6 via the 1-zigzagging 2-factorization (12)(34), which contains its 2-factors having exactly two consecutive edges in common with each 4-cycle, as shown in Fig. 2(e,f,g,j,b,c). In items 3(a-f), the non-egc cases indicated via “ \Leftrightarrow ” include those not satisfying the sufficient condition of Lemma 9, because such condition becomes also necessary for each Γ arising from a toroidal or Klein-bottle cutout as in Remarks 5–6. Moreover, all the 1-zigzagging cycles in Γ have even length and share two consecutive edges with each 4-cycle precisely where indicated via “ \Leftrightarrow ” in items 3(a-f). Furthermore, in Fig. 2(e,f,g,j), the thin diagonals separate those pairs of consecutive edges (for the 2-factorization (12)(34)), while the dashed ones do the same for the 2-factorization (14)(23). In addition, note the exclusion in item 3(a) of the cases $\{4, 4\}_{6, 1}^1$ and those for which $r = 3s + 1$, and in item 3(c) the case $\{4, 4\}_{6, 3}^1$. In item 3(b), note the lower bound for r , due to $\{4, 4\}_{8, 2}^4$ being a 3^22^2 -graph but not egc. For item 3(e), the case $s = 0$ is covered in item 2(a).

For the cases of Klein-bottle graphs in item 3(f), there are two different color patterns, the first one, exemplified in Fig. 2(b), valid for $6 \leq r \in 2\mathbb{Z}$ and the second one further restricted to having $r \in 4\mathbb{Z}$, with more than two colors on each horizontal line. Note the exclusion of the cases $[4, 4]_{4, t}^0$ ($3 < t \in \mathbb{Z} \setminus 2\mathbb{Z}$), for they are not girth-regular. \square

The egc-cases of Theorem 10 item 3 are exemplified respectively in Fig. 2(e,f,g,j,b,c), characterized by having cycles with blue-hazel horizontal edges and cycles with red-green non-horizontal edges. However, transposing the two colors in 1-zigzagging cycles of 2-factors in 2-factorizations (12)(34), (13)(24) or (14)(23) yield tight factorizations with horizontal cycles colored with more than 2 colors.

3.1 The 4-cube as a twice-egc girth-4-regular graph

Consider the three mutually orthogonal Latin squares of order 4, or MOLS(4) [3] contained as the second, third and fourth rows in the following compound matrix:

	1	2	4	7	
0	111	222	333	444	
3	243	134	421	312	(1)
5	324	413	142	231	
6	432	341	214	123	

where row/column headings (with/without apostrophe) stand for the following 4-tuples:

$$\begin{aligned}
 0 &= 0000, & 1 &= 1000, & 2 &= 0100, & 3 &= 1100, & 4 &= 0010, & 5 &= 1010, & 6 &= 0110, & 7 &= 1110, \\
 0' &= 0001, & 1' &= 1001, & 2' &= 0101, & 3' &= 1101, & 4' &= 0011, & 5' &= 1011, & 6' &= 0111, & 7' &= 1111.
 \end{aligned}
 \tag{2}$$

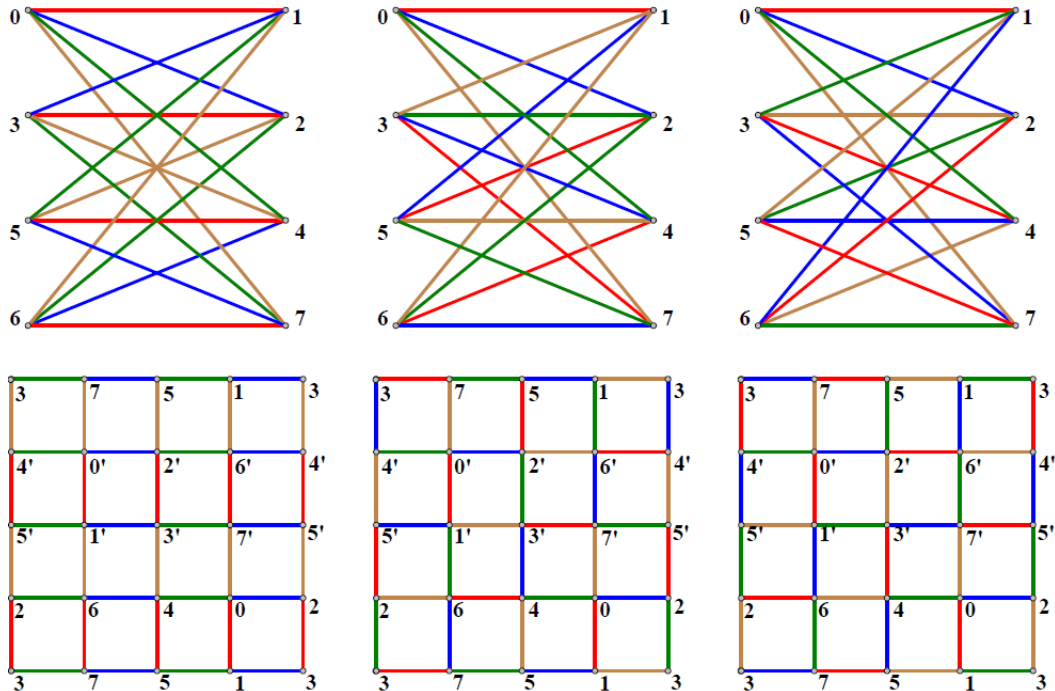


Figure 3: Factors of $K_{4,4}$ and toroidal cutouts of Q_4 with 0-, 1- and 2-color 4-cycles.

Based on display (1), the top of Fig. 3 contains three copies of $K_{4,4}$ properly colored in a mutually-orthogonal way, where colors are numbered as at the end of Remark 5. Letting

$\phi : Q_4 \rightarrow K_{4,4}$ be the canonical projection map of Q_4 seen as a double covering of $K_{4,4}$ obtained by identifying the pairs of antipodal vertices of $Q_4 = \{4, 4\}_{4,4}^0$, these vertices denoted as in display (2), note that in the bottom of Fig. 3 corresponding copies of the colored inverse images $\phi^{-1}(K_{4,4})$ of the three mentioned copies of $K_{4,4}$ are depicted. The leftmost copy of Q_4 in Fig. 3 has color i attributed precisely to those edges parallel to the i^{th} coordinate direction, for $i = 1, 2, 3, 4$. This constitutes a 1-factorization $F_0 = \{F_0^1, F_0^2, F_0^3, F_0^4\}$ of Q_4 . On the other hand, the center and rightmost copies of Q_4 in the figure determine 1-factorizations F_1 and F_2 of Q_4 for which each girth cycle of Q_4 intersects every composing 1-factor F_i^j of F_i , where $i = 1, 2$ and $j = 1$ (red), 2 (blue), 3 (green), 4 (hazel).

For each edge e of Q_4 , we say that e has i -color $j \in \{1, 2, 3, 4\}$ if $e \in F_i^j$. Then, each 4-cycle of Q_4 has opposite edges with a common 0-color in $\{1, 2, 3, 4\}$, with a total of two (nonadjacent) 0-colors in $\{1, 2, 3, 4\}$ per 4-cycle, say 0-colors $\ell_1, \ell_2 \in \{1, 2, 3, 4\}$, with $\ell_1 \neq \ell_2$, so one such 4-cycle can be expressed as $(\ell_1, \ell_2, \ell_1, \ell_2)$. On the other hand, the 4-cycles of Q_4 use all four i -colors 1,2,3,4, once each, for $i = 1, 2$.

There are twenty-four 4-cycles in Q_4 , six of each of the 0-color 4-cycles expressed in the first two columns of the following array, with two complementary 0-color 4-cycles per row. On the other hand, the third and fourth columns here contain respectively the 1-color and 2-color 4-cycles corresponding to the 0-color 4-cycles in the first two columns:

$$\begin{array}{|c|c|c|c|} \hline (1212) & (3434) & (1234) & (1243) \\ \hline (1313) & (2424) & (1324) & (1342) \\ \hline (1414) & (2323) & (1423) & (1432) \\ \hline \end{array} \quad (3)$$

3.2 Toroidal representation tables

Remark 11. The triple array in Table 1 presents F_i ($i = 0, 1, 2$) in schematic representations of $Q_4 = \{4, 4\}_{4,4}^0$, where \circ stands for a vertex of Q_4 and \square stands for an i -color 4-cycle. This table guarantees Theorem 10 item 3(c) via the last two columns of color quadruples in display (3), because the four colors are employed on the edges of each 4-cycle:

\circ	3	\circ	2	\circ	3	\circ	2	\circ	\circ	1	\circ	3	\circ	2	\circ	4	\circ	\circ	2	\circ	1	\circ	4	\circ	3	\circ
4	\square	4	\square	4	\square	4	\square	4	2	\square	4	\square	1	\square	3	\square	2	1	\square	4	\square	3	\square	2	\square	1
\circ	3	\circ	2	\circ	3	\circ	2	\circ	\circ	3	\circ	2	\circ	4	\circ	1	\circ	\circ	3	\circ	2	\circ	1	\circ	4	\circ
1	\square	1	\square	1	\square	1	\square	1	4	\square	1	\square	3	\square	2	\square	4	2	\square	1	\square	4	\square	3	\square	2
\circ	3	\circ	2	\circ	3	\circ	2	\circ	\circ	2	\circ	4	\circ	1	\circ	3	\circ	\circ	4	\circ	3	\circ	2	\circ	1	\circ
4	\square	1	\square	4	\square	1	\square	4	1	\square	3	\square	2	\square	4	\square	1	3	\square	2	\square	1	\square	4	\square	3
\circ	3	\circ	2	\circ	3	\circ	2	\circ	\circ	4	\circ	1	\circ	3	\circ	2	\circ	\circ	1	\circ	4	\circ	3	\circ	2	\circ
1	\square	1	\square	1	\square	1	\square	1	3	\square	2	\square	4	\square	1	\square	3	4	\square	3	\square	2	\square	1	\square	4
\circ	3	\circ	2	\circ	3	\circ	2	\circ	\circ	1	\circ	3	\circ	2	\circ	4	\circ	\circ	2	\circ	1	\circ	4	\circ	3	\circ

Table 1: Representations of F_i ($i = 0, 1, 2$).

- (a) either as horizontal or vertical color quadruples (as in display 3) alternated with the symbols \circ that represent the vertices of Q_4 ;
- (b) or as quadruples around the symbols \square representing the other 4-cycles.

00	2	01	4	02	1	03	3	04	2	05	00	2	01	1	02	3	03	4	04	2	05	1	06	3	07
1	\square	3	\square	2	\square	4	\square	1	\square	3	1	\square	3	\square	4	\square	2	\square	1	\square	3	\square	4	\square	2
05	4	06	1	07	3	08	2	09	4	10	07	4	08	2	09	1	10	3	11	4	12	2	13	1	14
3	\square	2	\square	4	\square	1	\square	3	\square	2	2	\square	1	\square	3	\square	4	\square	2	\square	1	\square	3	\square	4
10	1	11	3	12	2	13	4	14	1	15	14	3	15	4	16	2	17	1	18	3	19	4	20	2	21
2	\square	4	\square	1	\square	3	\square	2	\square	4	4	\square	2	\square	1	\square	3	\square	4	\square	2	\square	1	\square	3
15	3	16	2	17	4	18	1	19	3	00	21	1	22	3	23	4	24	2	25	1	26	3	27	4	00
4	\square	1	\square	2	\square	3	\square	4	\square	1	3	\square	4	\square	2	\square	1	\square	3	\square	4	\square	2	\square	1
00	2	01	4	02	1	03	3	04	2	05	00	2	01	1	02	3	03	4	04	2	05	1	06	3	07

Table 2: Distinction of the two cases F_1 and F_2 .

By associating the oriented quadruple $(1,3,2,4)$ (resp. $(3,4,1,2)$) of successive edge colors on the left-to-right and the downward (resp. the right-to-left and the downward) straight paths in F_1 (resp. F_2), situations that we indicate by “ $\searrow (1, 3, 2, 4)$ ” (resp. “ $\swarrow (3, 4, 1, 2)$ ”), a complete invariant for F_1 (resp. F_2) is obtained that we denote by combining between square brackets the just presented notations:

$$[a_{\swarrow 12,34}, b_{\searrow 13,24}, \searrow (1, 3, 2, 4)], \text{ (resp. } [a_{\searrow 13,24}, b_{\swarrow 12,34}, \swarrow (3, 4, 1, 2)]).$$

This invariant distinguishes F_1 and F_2 from each other and is generalized for the toroidal graphs in Theorem 10, as we will see below in this subsection.

Table 1 is also presented to establish similar patterns, like in Table 2, allowing in a likewise manner to guarantee Theorem 10 item 2(b). We say that

1. F_1 has $a_{\swarrow 12,34}$ -zigzags if any 1-zigzagging path obtained by walking left, down, left, down and so on, alternates either colors 1 and 2, or colors 3 and 4;
2. F_1 has $b_{\searrow 13,24}$ -zigzags if any 2-zigzagging path obtained by walking right, right, down, down and so on, alternates either colors 1 and 3, or colors 2 and 4;
3. F_2 has $a_{\searrow 13,24}$ -zigzags if any 2-zigzagging path obtained by walking left, left, down, down and so on, either alternates colors 1 and 2, or colors 3 and 4;
4. F_2 has $b_{\swarrow 12,34}$ -zigzags if any 1-zigzagging path obtained by walking right, down, right, down and so on, either alternates colors 1 and 3, or colors 2 and 4.

A representation as in Table 1 may be used for the graphs in items 1(b) and 2 of Theorem 10. For example, the cases $(r, t, s) = (20, 1, 5)$ and $(r, t, s) = (28, 1, 5)$ in Fig. 2(h-i) are representable as in Table 2, where, instead of \circ standing for each vertex, we set the vertex

notation of Fig. 2(h-i). Here the four colors are indicated as in Fig. 2(d-j) and Subsection 3.1. To distinguish the two cases in Table 2, note that the 4-cycles of $\{4, 4\}_{20,1}^5$ (resp. $\{4, 4\}_{28,1}^5$) have the 2-factors by color pairs $\{1, 2\}$ and $\{3, 4\}$ descending in zigzag from right to left (resp. left to right), by alternate vector displacements $(-1, 0)$ (resp. $(1, 0)$) for colors 1 and 3, and $(0, -1)$ for colors 2 and 4. Generalizing and using the invariant notation of Remark 11, we can say that the egc graphs in item 2(b) of Theorem 10 are as follows:

1. $\{4, 4\}_{6x+2,1}^5$ for $x > 2$ has invariant $[a_{\swarrow 12,34}, b_{\searrow 13,24}, \searrow (2, 4, 1, 3)]$;
2. $\{4, 4\}_{6x+4,1}^5$ for $x > 2$ has invariant $[a_{\swarrow 13,24}, b_{\searrow 12,34}, \swarrow (2, 4, 3, 1)]$.

As in Remark 11, we have here a distinguished oriented slanted arrow triple: either $[\swarrow, \searrow, \searrow]$ or $[\searrow, \swarrow, \swarrow]$. The graphs in item 2 of Theorem 10 admit both invariants.

3.3 The bipartite complement of the Heawood graph

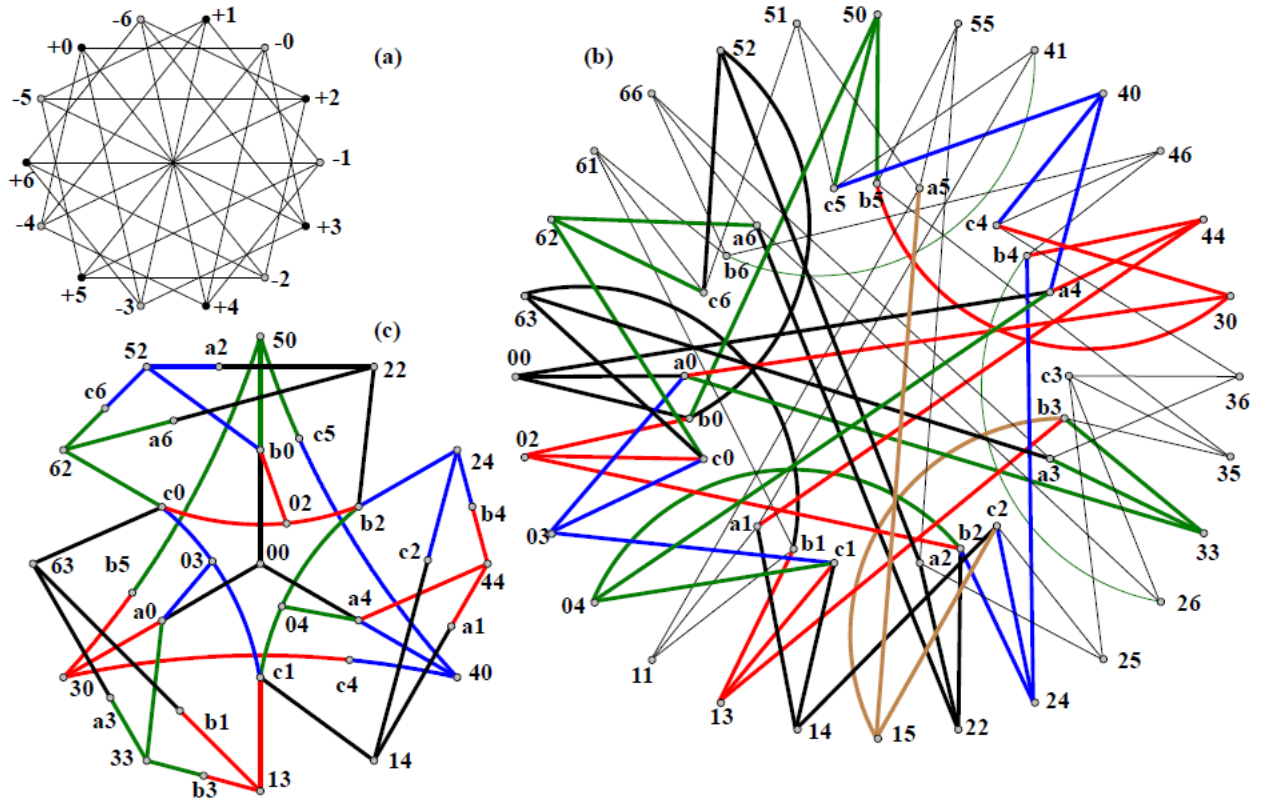


Figure 4: Bipartite complement H of the Heawood-graph and associated graph $GA(H)$.

The bipartite complement H of the Heawood-graph, with vertex set $V(H) = \{ij; i \in \{+, -\}, j \in \mathbb{Z}_7\}$, is depicted on the upper left of Fig. 4; its edges $\{+j, -j\}$, $\{+j, -(j+2)\}$, $\{+j, -(j+3)\}$ and $\{+j, -(j+4)\}$, for $j \in \mathbb{Z}_7$, will be denoted jj , $j(j+2)$, $j(j+3)$ and $j(j+4)$, respectively, where addition is taken (mod 7). This yields the twenty-eight edges of

$a_0 = (00, 30, 33, 03),$	$b_0 = (00, 50, 52, 02),$	$c_0 = (02, 62, 63, 03),$
$a_1 = (11, 41, 44, 14),$	$b_1 = (11, 61, 63, 13),$	$c_1 = (13, 03, 04, 14),$
$a_2 = (22, 52, 55, 25),$	$b_2 = (22, 02, 04, 24),$	$c_2 = (24, 14, 15, 25),$
$a_3 = (33, 63, 66, 36),$	$b_3 = (33, 13, 15, 35),$	$c_3 = (35, 25, 26, 36),$
$a_4 = (44, 04, 00, 40),$	$b_4 = (44, 24, 26, 46),$	$c_4 = (46, 36, 30, 40),$
$a_5 = (55, 15, 11, 51),$	$b_5 = (55, 35, 30, 50),$	$c_5 = (50, 40, 41, 51),$
$a_6 = (66, 26, 22, 62),$	$b_6 = (66, 46, 41, 61),$	$c_6 = (61, 51, 52, 62).$

Table 3: The twenty-one 4-cycles a_i, b_i, c_i of H ($i \in \mathbb{Z}_7$).

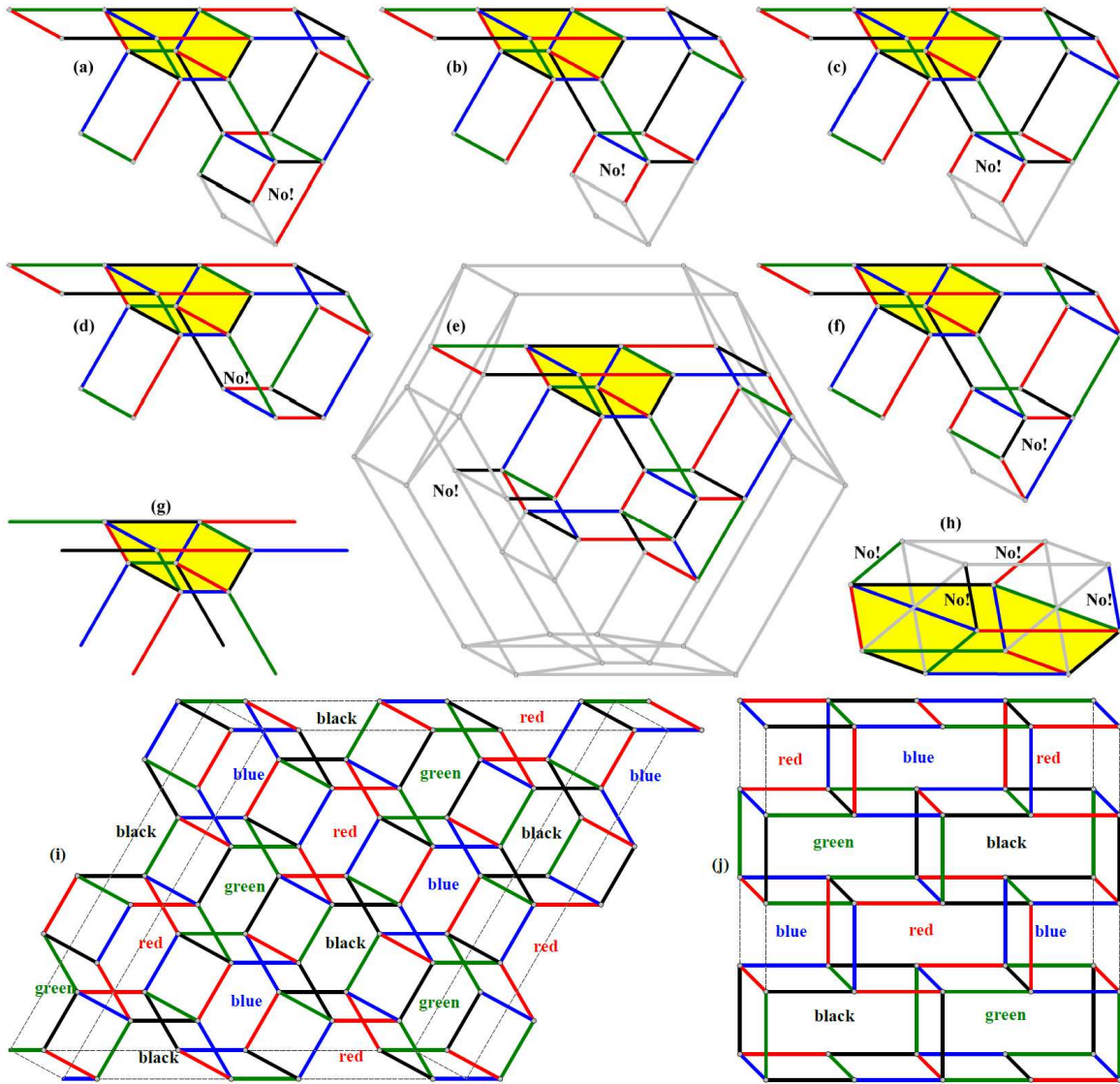


Figure 5: Prisms of: truncated octahedron (32^2_1), $K_{3,3}$ (4^3_3), ST_4 and 16-vertex graph (31^3).

H as arcs from $+$ to $-$ vertices. They form twenty-one 4-cycles a_i, b_i, c_i ($i \in \mathbb{Z}_7$) expressed, by omitting the signs \pm , as in Table 3.

This way, $j_j = a_j \cap a_{j+4} \cap b_j$, $j(j+2) = b_j \cap b_{j+2} \cap c_j$, $j(j+3) = a_j \cap c_j \cap c_{j+1}$ and $j(j+4) = a_{j+4} \cap b_{j+2} \cap c_{j+1}$, $\forall j \in \mathbb{Z}_7$. We show there is no proper edge coloring of H that is tight on every 4-cycle. To prove this, we recur to the bipartite graph $\text{GA}(H)$ whose parts V_1 and V_2 are respectively the twenty-eight edges of H and the twenty-one 4-cycles of H , with adjacency between an edge ij of H and a 4-cycle C of H whenever C passes through ij ; $\text{GA}(H)$ is represented in Fig. 4(b) with a_i written as ai ($i = 1, 2, 3$). A tight factorization of H would be equivalent to a 4-coloring of $\text{GA}(H)$ that is monochromatic on each vertex of V_1 but covering the four colors at the edges incident to each vertex of V_2 . We begin by coloring the edges incident to vertices 00, 02, 03, 04 respectively with colors black, red, blue and green. This forces the coloring of the subgraph of $\text{GA}(H)$ in the lower left of Fig. 4. By transferring this coloring to the representation of $\text{GA}(H)$ on the right of Fig. 4, as shown, it is verified that vertex 15 on the bottom of the representation does not admit properly any of the four used colors.

4 Prisms of types 4443, 3221 and 3221

Given a graph Γ' , the prism graph $\text{Prism}(\Gamma')$ of Γ' is the graph cartesian product $K_2 \square \Gamma'$. The cases of $(e_1)(e_2)(e_3)(e_4)$ -graphs with $(e_1)(e_2)(e_3)(e_4) \neq 1^4$, apart from those treated in Section 3, are the prisms $\Gamma = \text{Prism}(\Gamma')$ of $(e_1)(e_2)(e_3)$ -graphs Γ' . It is easy to see that there is no egc graph Γ if $g(\Gamma')$ is odd.

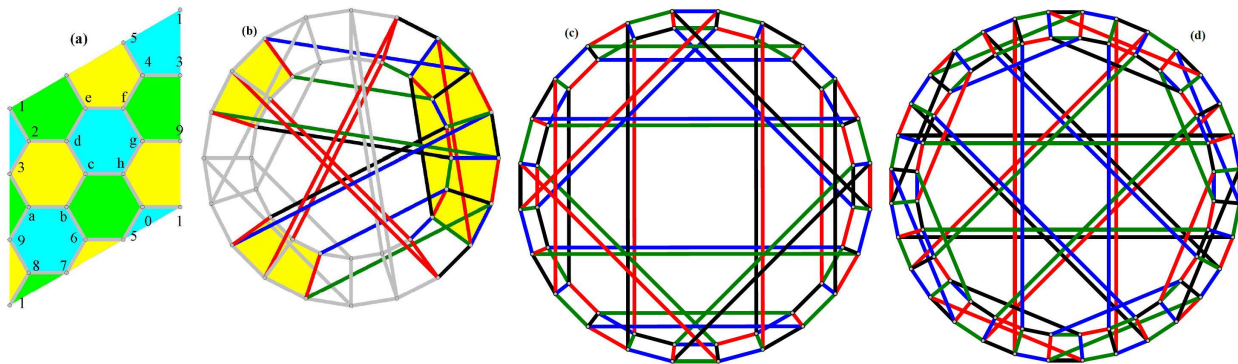


Figure 6: A Pappus-graph cutout and the Desargues, Nauru and Dyck graph prisms.

Conjecture 12. Graphs Γ with signatures 32^21 and 4^33 are not egc.

Example 13. Conjecture 12 is sustained by the exhaustive partial colorings of the prisms of the 24-vertex truncated octahedral graph [8, pp. 79–86] in Fig. 5(a–g) and of the 6-vertex Thomsen graph $K_{3,3}$ [7] in Fig. 5(h), which are respectively a 32^21 -graph and a 4^33 -graph, with the incidental obstructions indicated by a notification "No!" in each case. Such exhaustive partial colorings can be found similarly for example in the 120-vertex truncated-icosidodecahedral graph [8, pp. 97–99].

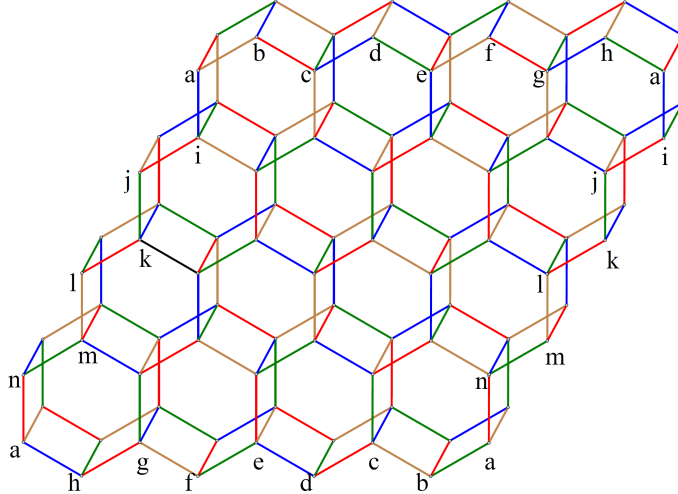


Figure 7: An edge-girth coloring of the prism of $\{6, 3\}_{|4,4}$ on the Klein bottle.

Remark 14. A 31^3 -graph $\Gamma = K_2 \square \Gamma'$, where Γ' is a toroidal quotient graph of the hexagonal tessellation [4, 5] (i.e. the tiling of the plane with Schläfli symbol $\{6, 3\}$), may be an egc 31^3 -graph. This is exemplified in Fig. 5(i–j), namely for the prisms of the 24-vertex star graph ST_4 (with twelve girth 6-cycles) [9] and a 16-vertex graph (with just eight girth 6-cycles). But Γ' cannot be the Pappus graph. Let us see why. A cutout in this case, as in Fig. 6(a) (with octodecimal vertex notation and proper face coloring) contains nine hexagonal tiles. In order to use the specified coloring to guarantee the existence of an egc-graph, the “period” employed when moving from any particular vertex v_R of a cutout R in any of the three directions perpendicular to the edges of the tessellation – i.e., the number of tiles met until a similar vertex $v_{R'}$ in a cutout R' adjacent to R is reached – must be even, but 9 is odd, leading to a contradiction.

Remark 15. In the setting of Remark 14, by considering the junction of three hexagonal prisms P_1, P_2, P_3 , it is seen that in any such P_i ($i = 1, 2, 3$), two edges not belonging to a hexagon can only be of the same color if their endpoints are antipodal in the two hexagons of P_i . Up to automorphism and permutation of colors, this allows for two distinct colorings of the hexagonal prisms:

1. the one as in both instances of Fig. 5(i–j) (with one color appearing on six edges and the remaining four colors appearing each on four edges), and
2. one with two colors appearing each on five edges and the other two colors appearing each on four edges.

See Fig. 7, depicting a cutout of an egc-graph on the Klein bottle, namely an edge-girth coloring of the prism of $\{6, 3\}_{|4,4}$ [23] on the Klein bottle. In Fig. 7, the colorings of the hexagonal prisms in which one color appears six times only occur in the first row, and no edge-girth coloring of this graph is possible if only such colorings are used. Computational evidence has been obtained that gives support to the following conjectures.

Conjecture 16. The condition of even periods in Remark 14 is sufficient for the case of prisms of hexagonal tessellations of the torus.

Conjecture 17. The prisms of the hexagonal tessellations of the Klein bottle [23] are egc if the cutout contains $m \times n$ tiles, with m and n even, and having both types of colorings of the hexagonal prism as in Remark 15.

Example 18. Conjecture 17 is sustained by the prism cutout in Fig. 7, showing an edge-girth coloring of the prism of $\{6, 3\}_{|4;4|}$ [23] on the Klein bottle. Note that the colorings of the hexagonal prisms in which one color appears six times only occur in the first row, and no edge-girth coloring of this graph is possible if only such colorings are used.

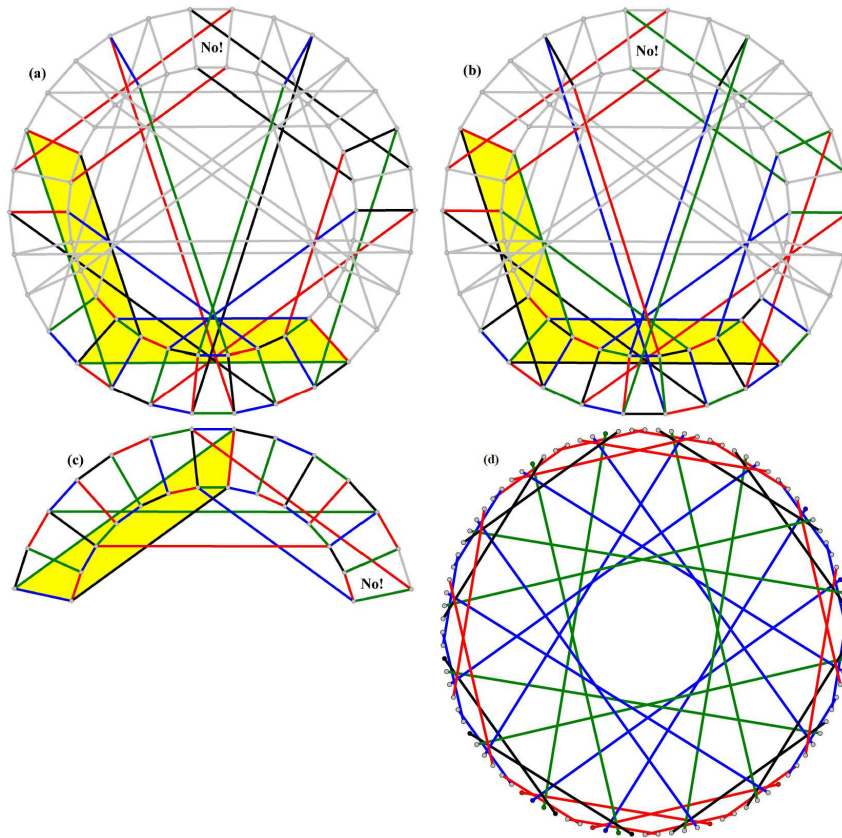


Figure 8: Tutte 8-cage 31^3 -graph prism and 96-vertex cubic Γ' .

Example 19. In Fig. 6(b), the prism of the Desargues graph on twenty vertices is shown non-egc via obstructions by pairs of forced “long” parallel red edges. However, in Fig. 6(c–d) the Nauru and Dyck graphs on twenty-four and thirty-two vertices, respectively, are shown to have their prisms as egc graphs by means of corresponding tight factorizations.

Example 20. For the case $g(\Gamma') = 8$, let us consider Γ' to be the Tutte 8-cage on 30 vertices. Fig. 8(a–c) shows why its 31^3 -graph prism is not egc, with five 8-cycle prisms $K_2 \square C_8$ in Γ

(presented cyclically mod 5), each of whose vertices should have its four incident edges colored differently. In fact, Fig. 8(a–c) presents exhaustively without loss of generality partial edge-colorings in Γ , with copies of $K_2 \square C_8$ edge-colored accordingly and notification “No!” if an obstruction to edge-coloring continuation appears.

$\bar{3}$	$\bar{3}$	4	1	2	3	$\bar{4}$	$\bar{3}$	4	2	1	3	$\bar{4}$	$\bar{4}$	3	2	1	4	$\bar{3}$	$\bar{4}$	3	1	2	4
$\circ 4$	$\circ 1$	$\circ 2$	$\circ 3$	$\circ 4$	$\circ 1$	$\circ 2$	$\circ 1$	$\circ 3$	$\circ 4$	$\circ 2$	$\circ 1$	$\circ 3$	$\circ 2$	$\circ 1$	$\circ 4$	$\circ 3$	$\circ 2$	$\circ 1$	$\circ 2$	$\circ 4$	$\circ 3$	$\circ 1$	$\circ 2$
$\square 1$	$\square 2$	$\square 3$	$\square 4$	$\square 1$	$\square 2$	$\square 3$	$\square 4$	$\square 2$	$\square 1$	$\square 3$	$\square 4$	$\square 2$	$\square 1$	$\square 4$	$\square 3$	$\square 2$	$\square 1$	$\square 4$	$\square 3$	$\square 1$	$\square 2$	$\square 4$	$\square 3$
$\circ 3$	$\circ 4$	$\circ 1$	$\circ 2$	$\circ 3$	$\circ 4$	$\circ 1$	$\circ 3$	$\circ 4$	$\circ 2$	$\circ 1$	$\circ 3$	$\circ 4$	$\circ 3$	$\circ 2$	$\circ 1$	$\circ 4$	$\circ 3$	$\circ 2$	$\circ 4$	$\circ 3$	$\circ 1$	$\circ 2$	$\circ 4$
$\bar{2}$	$\bar{1}$	2	3	4	1	$\bar{2}$	$\bar{2}$	1	3	4	2	$\bar{1}$	$\bar{2}$	1	4	3	2	$\bar{1}$	$\bar{1}$	2	4	3	1

Table 4: Representing a coloring of 8-cycle prisms Θ_i ($i = 1, 2, 3, 4$).

On the other hand, Table 4 uses the notation of Table 1 in representing a coloring of the union U of almost four (namely $3\frac{3}{4}$) contiguous 8-cycle prisms Θ_i ($i = 1, 2, 3, 4$) and the resulting forced colors for the departing edges away from U . In Table 4, the middle row sequence, call it Υ , (obtained by disregarding the symbols “ \square ”, or replacing them by commas) represents the subsequences of colors of the edges $\{(0, u), (1, u)\}$ in the prisms Θ_i , namely the subsequences $\Upsilon_1 = (1, 2, 3, 4)^2$, $\Upsilon_2 = (3, 4, 2, 1)^2$, $\Upsilon_3 = (2, 1, 4, 3)^2$ and $\Upsilon_4 = (4, 3, 1, 2)^2$. Here, the last two terms of each Υ_i coincide (i.e. are shared) with the first two terms of its subsequent Υ_{i+1} , where the last 6-term subsequence is completed to Υ_4 by adding the first two terms of Υ_1 , so Υ_1 may be considered as the next Υ_i after the last Υ_4 (and explaining the fraction $3\frac{3}{4}$ mentioned above). This suggest that Υ can be concatenated with itself a number ℓ of times to close a $(24 \times \ell)$ -cycle of colors for the edges $(\{0, u), (1, u)\}$ of a Hamilton-cycle (of Γ') prism H which may be completed to an egc graph Γ by means of the following considerations. (An adequately colored graph Γ' is obtained from Fig. 8(d) by adding a suitable colored outer cycle, missing in the figure).

On the top and bottom rows of Table 4, the colors 1, 2, 3 and 4 with a bar on top are those of the “long” edges in the four prisms Θ_i that close the two 8-cycles in each Θ_i . The remaining (non-barred) colors suggest that the corresponding edges form external 4-cycles that may be joined with H to form a Γ as desired. The “even longer” edges of these external 4-cycles must be set to form (with two edges of the form $\{(0, u), (1, u)\}$) new 4-cycles and can be selected to form the desired Γ by taking the number of concatenated copies of U to be $\ell = 4$, so that $|V(\Gamma)| = 192$. The two columns in Table 4 whose transpose rows are “ $4 \circ 3 \circ 2$ ” and “ $4 \circ 1 \circ 2$ ”, namely the third leftmost and seventh rightmost \square -free columns, integrate one such 4-cycle. The leftmost third, fourth, fifth and sixth columns are paired this way with the rightmost seventh, eighth, ninth and tenth columns, but the last three pairs must be paired with similar columns in the second, third and fourth version of Table 4 (for indices $k \in \{2, 3, 4 = \ell\}$ of copies U_k of U , if we agree that the leftmost third and rightmost seventh columns above are both for $k = 1$ and $U = U_k = U_1$). The same treatment can be set from the leftmost ninth, tenth, eleventh and twelfth respectively to the rightmost first, second, third and fourth columns, which also correspond in pairs that form again “long” 4-cycles.

Theorem 21. For each $4 \leq k \in \mathbb{Z}$, there is an egc 31^3 -graph Γ with $192 \times k$ edges as a prism of a hamiltonian cubic graph Γ' on $96 \times k$ vertices based on g contiguous copies of the edge-colored subgraph in Table 4. However, the Tutte 8-cage is a non-egc 31^3 -graph.

Proof. The argument above the statement can be completed for the case $k = 1$. By concatenating the graph from Table 4 any multiple of g times, one extends the construction. \square

Remark 22. The cubic vertex-transitive graphs on less than one hundred vertices with girth 10 and that have egc prisms are in the notation of [16]:

CubicVT[80,30], CubicVT[96,34], CubicVT[96,49], CubicVT[96,50] and CubicVT[96,62].

5 EgC 1111-graphs

A construction [24] of 1^4 -graphs, also called *girth-tight* [18], proceeds as follows. Let Γ be 4-regular and let \mathcal{C} be a partition of $E(\Gamma)$ into cycles. The pair (Γ, \mathcal{C}) is a *cycle decomposition* of Γ . Two edges of Γ are *opposite* at vertex v if both are incident to v and belong to the same element of \mathcal{C} . The *partial line graph* $\mathbb{P}(\Gamma, \mathcal{C})$ of (Γ, \mathcal{C}) is the graph with the edges of Γ as vertices, and any two such vertices adjacent if they share, as edges, a vertex of Γ and are not opposite at that vertex. A cycle C in Γ is \mathcal{C} -*alternating* if no two consecutive edges of C belong to the same element of \mathcal{C} . Lemma 4.10 [18] says that $\mathbb{P}(\Gamma, \mathcal{C})$ is girth-tight if and only if (Γ, \mathcal{C}) contains neither \mathcal{C} -alternating cycles nor triangles, except those contained in \mathcal{C} .

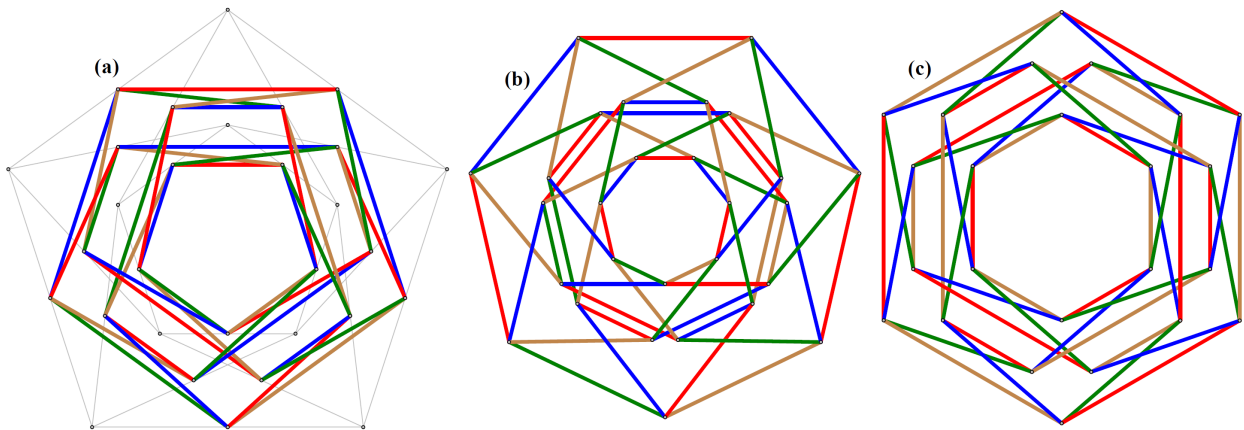


Figure 9: Tight factorizations of $\mathbb{P}(W(5, 2))$, $\mathbb{P}(W(7, 2))$ and $\mathbb{P}(W(6, 2))$.

Example 23. As initial example of a partial line graph, consider the wreath graph $W(n, 2) = C_n[\overline{K_2}]$ ($n > 4$), where C_n is a cycle $(v_0, v_1, \dots, v_{n-1})$. Consider the partition \mathcal{C} of $W(n, 2)$ into the 4-cycles $((v_i, 0), (v_{i+1}, 0), (v_i, 1), (v_{i+1}, 1))$ ($i \in \mathbb{Z}_n$). These form a decomposition $(W(n, 2), \mathcal{C})$, which yields the partial line graph $\mathbb{P}(W(n, 2), \mathcal{C})$. We prove now that for all values of n , $\mathbb{P}(W(n, 2), \mathcal{C})$ is egc, as in Fig. 9(a–c), where $\mathbb{P}(W(5, 2), \mathcal{C})$, $\mathbb{P}(W(7, 2), \mathcal{C})$ and $\mathbb{P}(W(6, 2), \mathcal{C})$ are represented, showing tight factorizations via edge colors 1, 2, 3, 4.

Theorem 24. Let $4 < n \in \mathbb{Z}$. Then, $\mathbb{P}(W(n, 2), \mathcal{C})$ is egc.

Proof. Each vertex $((v_i, j)(v_{i\pm 1}, j'))$ of $\mathbb{P}(W(n, 2), \mathcal{C})$ representing the edge between the vertices (v_i, j) and $(v_{i\pm 1}, j')$ of $W(n, 2)$, where $i \in \mathbb{Z}_n$ and $j, j' \in \{0, 1\}$, will be denoted $(i_j(i \pm 1)_{j'})$. We use modifications of Lemma 9 separately for the cases of odd and even n . If $n = 2k + 1$ is odd, then we have a 2-factorization of $\mathbb{P}(W(n, 2), \mathcal{C})$, one of whose two 2-factors is composed by three disjoint even-length cycles not sharing more than two edges with any 4-cycle, namely one of length 8 and two of length $4k + 2$, specifically

$$\begin{aligned} &((-k_0k_0)(-k_0(1-k)_1)(-k_0k_1)((k-1)_0k_1)(-k_1k_1)(-k_1(1-k)_0)(-k_1k_0)((k-1)1k_0)); \\ &((-k_0(1-k)_0) \cdots (-1_00_0)(0_01_0) \cdots ((k-1)_0k_0)(k_0(k-1)_1) \cdots (1_10_1)(0_1-1_1) \cdots (k_1-k_0)); \\ &((-k_1(1-k)_1) \cdots (-1_10_1)(0_11_1) \cdots ((k-1)_1k_1)(k_1(k-1)_0) \cdots (1_00_0)(0_0-1_0) \cdots (k_0-k_1)), \end{aligned}$$

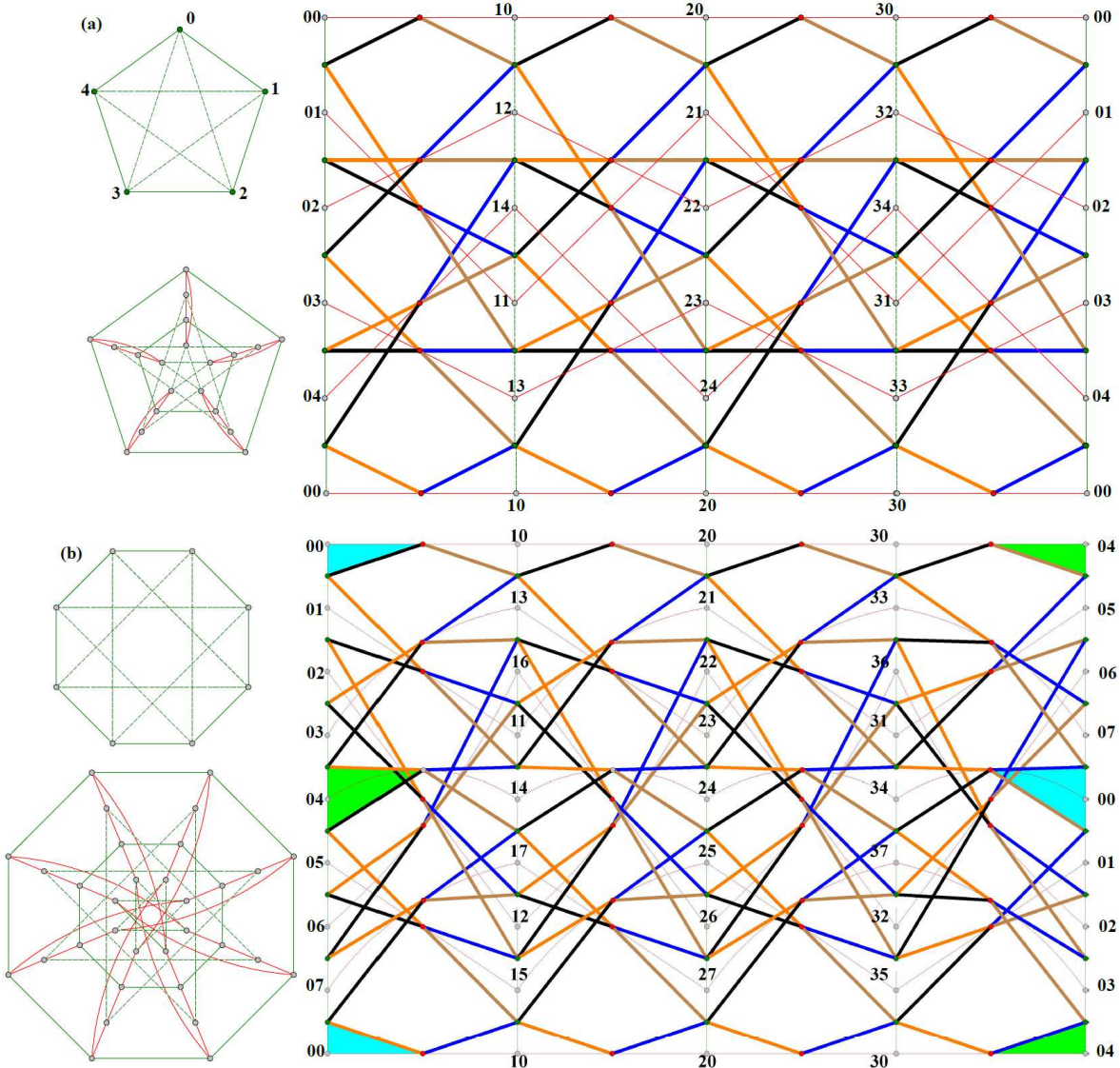


Figure 10: Tight factorizations of (a) $\mathbb{P}(\text{Br}(4, 5; 2))$ and (b) $\mathbb{P}(\text{MBr}(4, 8; 3))$.

which for $k = 2$ and $k = 3$ can be visualized respectively in Fig. 9(a) and Fig. 9(b) as three alternate-red-blue cycles, one of length 8 and two of length $4k + 2$. The other 2-factor

also is formed by even cycles not sharing more than two edges with any 4-cycle, viewable as alternate-green-hazel cycles for $k = 2$ in Fig. 9(a) and for $k = 3$ in Fig. 9(b). This 2-factor has reflective \mathbb{Z}_2 symmetry on a vertical axis. As for the mentioned modifications of Lemma 9, note that the two cycles of length $4k + 2$ differ, either for k odd or for k even differ: If k is odd, the two cycles of length $2k + 2$ contain opposite edges in the 4-cycles, while if k is even, the two cycles of length $2k + 2$ share just one edge with each 4-cycle. Both cases refine into corresponding tight 1-factorizations. In particular, if $n = 2k$ is even, then a 2-factorization of $\mathbb{P}(W(n, 2), \mathcal{C})$ is formed by k cycles of length 8 forming a class of cycles (mod k), namely

$$((i_0(i+1)_0)((i+1)_0(i+2)_0)((i+2)_0(i+1)_1)((i+1)_1 i_0)((i+1)_1 i_1)((i+1)_1(i+2)_1)((i+2)_1(i+1)_0)((i+1)_0 i_1)),$$

where i is odd, $0 < i < n$. The other 2-factor also is formed by 8-cycles, see Fig. 9(c). \square

In order to obtain additional girth-tight graphs with tight factorizations, we recur to a particular case of a cycle decomposition known as *linking-ring structure* [24], that works for two colors, say red and green. This structure applies in the following paragraphs only for n even; (if n is odd, then more than two colors would be needed in order to distinguish adjacent cycles of the decomposition $(W(n, 2), \mathcal{C})$). A *linking-ring structure* is defined in items (i)–(iii) below, as follows. An *isomorphism between two cycle decompositions* $(\Gamma_1, \mathcal{C}_1)$ and $(\Gamma_2, \mathcal{C}_2)$ is an isomorphism $\xi : \Gamma_1 \rightarrow \Gamma_2$ such that $\xi(\mathcal{C}_1) = \mathcal{C}_2$. An isomorphism ξ from a cycle decomposition to itself is an *automorphism*, written $\xi \in \text{Aut}(\Gamma, \mathcal{C})$. A cycle decomposition (Γ, \mathcal{C}) is *flexible* if for every vertex v and each edge e incident to v there is $\xi \in \text{Aut}(\Gamma, \mathcal{C})$ such that:

- (I) ξ fixes each vertex of the cycle in \mathcal{C} containing e and
- (II) ξ interchanges the two other neighbors of v ; the edges joining v to those neighbors are in some other cycle of \mathcal{C} .

A cycle decomposition (Γ, \mathcal{C}) is *bipartite* if \mathcal{C} can be partitioned into two subsets \mathcal{G} (green) and \mathcal{R} (red) so that each vertex of Γ is in one cycle of \mathcal{G} and one cycle of \mathcal{R} .

The largest subgroup of $\text{Aut}(\Gamma, \mathcal{C})$ preserving each of the sets $\mathcal{C}_1 = \mathcal{G}$, (\mathcal{G} for “green”), and $\mathcal{C}_2 = \mathcal{R}$, (\mathcal{R} for “red”), is denoted $\text{Aut}^+(\Gamma, \mathcal{C})$. In a bipartite cycle decomposition, an element of $\text{Aut}(\Gamma, \mathcal{C})$ either interchanges \mathcal{G} and \mathcal{R} or preserves each of \mathcal{G} and \mathcal{R} set-wise, so it is contained in $\text{Aut}^+(\Gamma, \mathcal{C})$. This shows that the index of $\text{Aut}^+(\Gamma, \mathcal{C})$ in $\text{Aut}(\Gamma, \mathcal{C})$ is at most 2. If this index is 2, then we say that (Γ, \mathcal{C}) is *self-dual*; this happens if and only if there is $\sigma \in \text{Aut}(\Gamma, \mathcal{C})$ such that $\mathcal{G}\sigma = \mathcal{R}$ and $\mathcal{R}\sigma = \mathcal{G}$. In [18], a cycle decomposition (Γ, \mathcal{C}) is said to be a *linking-ring (LR) structure* if it is

- (i) bipartite,
- (ii) flexible and
- (iii) $\text{Aut}^+(\Gamma, \mathcal{C})$ acts transitively on $V(\Gamma)$.

However, there are tight factorizations of girth-tight graphs $\mathbb{P}(\Gamma, \mathcal{P})$ obtained by relaxing condition (iii) in that definition. So we will say that a cycle decomposition (Γ, \mathcal{P}) is a *relaxed LR structure* if it satisfies just conditions (i) and (ii).

$(0_1^0[a]_1^0 1[b] 0_2^1[c]_0^3 1[d])$	$(1_2^0[a]_2^1 2[b] 1_4^2[c]_1^0 2[d])$	$(2_1^0[a]_3^2 1[b] 2_2^1[c]_2^1 1[d])$	$(3_2^0[a]_0^3 2[b] 3_4^2[c]_3^2 2[d])$
$(0_2^1[a]_1^0 2[b] 0_3^2[c]_0^3 2[d])$	$(1_3^1[a]_2^1 3[b] 1_0^3[c]_0^0 3[d])$	$(2_2^1[a]_3^2 2[b] 2_3^2[c]_2^1 2[d])$	$(3_3^1[a]_0^3 3[b] 3_0^3[c]_3^3 3[d])$
$(0_3^2[a]_1^0 3[b] 0_4^3[c]_0^3 3[d])$	$(1_4^2[a]_2^1 4[b] 1_1^4[c]_1^0 4[d])$	$(2_3^2[a]_3^3 3[b] 2_4^3[c]_2^1 3[d])$	$(3_4^2[a]_0^4 4[b] 3_1^4[c]_3^4 4[d])$
$(0_4^3[a]_1^0 4[b] 0_0^4[c]_0^3 4[d])$	$(1_0^3[a]_2^1 0[b] 1_2^0[c]_1^0 0[d])$	$(2_4^3[a]_3^4 4[b] 2_0^4[c]_2^1 4[d])$	$(3_0^3[a]_0^3 0[b] 3_2^0[c]_3^0 0[d])$
$(0_0^4[a]_1^0 0[b] 0_1^0[c]_0^3 0[d])$	$(1_1^4[a]_2^1 1[b] 1_3^1[c]_1^0 1[d])$	$(2_0^4[a]_3^0 0[b] 2_1^0[c]_2^1 0[d])$	$(3_1^0[a]_0^3 1[b] 3_3^1[c]_3^1 1[d])$

Table 5: A code representation of the tight factorization in Fig. 10(a).

Remark 25. With the aim of yielding semisymmetric graphs from LR structures, [24] defines:

- (a) the *barrel* $\text{Br}(k, n; r)$, where $4 \leq k \equiv 0 \pmod{2}$, $n \geq 5$, $r^2 \equiv \pm 1 \pmod{n}$, $r \not\equiv \pm 1 \pmod{n}$ and $0 \leq r < \frac{n}{2}$, as the graph with vertex set $\mathbb{Z}_k \times \mathbb{Z}_n$ and (i, j) red-adjacent to $(i \pm 1, j)$ and green-adjacent to $(i, j \pm r^i)$;
- (b) the *mutant barrel* $\text{MBr}(k, n; r)$, where $2 \leq k \equiv n \equiv 0 \pmod{2}$, $n \geq 6$, $r^2 \equiv \pm 1 \pmod{n}$ and $r \not\equiv \pm 1 \pmod{n}$, as the graph with vertex set $\mathbb{Z}_k \times \mathbb{Z}_n$ and (i, j) red-adjacent to $(i + 1, j)$ for $0 \leq i < k - 1$, $(k - 1, j)$ red-adjacent to $(0, j + \frac{n}{2})$, and (i, j) green-adjacent to $(i, j \pm r^i)$.

The right side of Fig. 10(a) (resp. 10(b)) represents $\mathbb{P}(\text{Br}(4, 5; 2))$ (resp. $\mathbb{P}(\text{MBr}(4, 8; 3))$), where: **(i)** each vertex (i, j) is denoted ij , **(ii)** vertices $i0$ appear twice (on top and bottom, to be identified for each i), **(iii)** red edges are shown in thin trace, **(iv)** green edges arising from the cycles $F_1^5 = (0, 1, 2, 3, 4)$ and $F_2^5 = (0, 2, 4, 1, 3)$ of K_5 (resp. $F_1^8 = (0, 1, 2, 3, 4, 5, 6, 7)$ and $F_3^8 = (0, 3, 6, 1, 4, 7, 2, 5)$ of K_8) are shown in thin and dashed trace, respectively, and **(v)** the edges of the corresponding partial line graphs are shown in thick trace on the colors orange = a , black = b , hazel = c and blue = d , setting a tight factorization.

Vertices of green and red cycles are said to be *green* and *red*, respectively. To the left of these two graphs in Fig. 10, the corresponding green and red-green subgraphs are shown.

Note that thick edges of colors orange and black form cycles zigzagging between:

- (A) the vertices of each vertical green cycle (excluding the rightmost green cycle) and
- (B) their adjacent red vertices to their immediate right.

Also, note that thick blue and hazel edges form cycles zigzagging between:

- (C) the red vertices and
- (D) the vertices of the next vertical green cycle to their right.

The girth is realized by 4-cycles with the four colors, with a pair of edges (blue and hazel) to the left of each vertical green cycle and another pair of edges (black and orange) to the corresponding right. This is always attainable, because similar bicolored cycles can always be obtained, generating the desired tight factorizations. For instance, assigning colors a, b, c, d

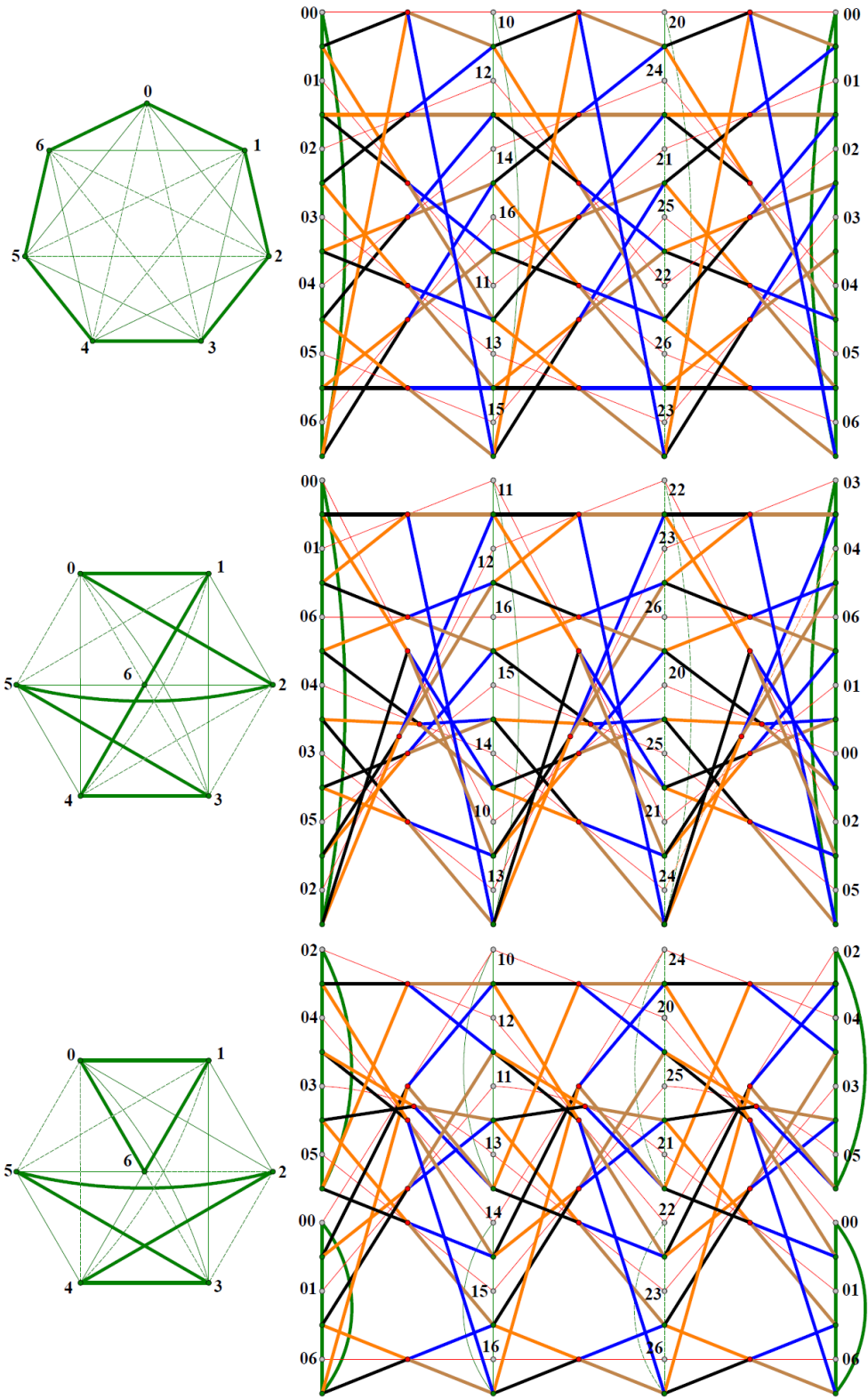


Figure 11: Egc $\mathbb{P}(\text{Br}(3, F))$ for the three 2-factorizations F of K_7 .

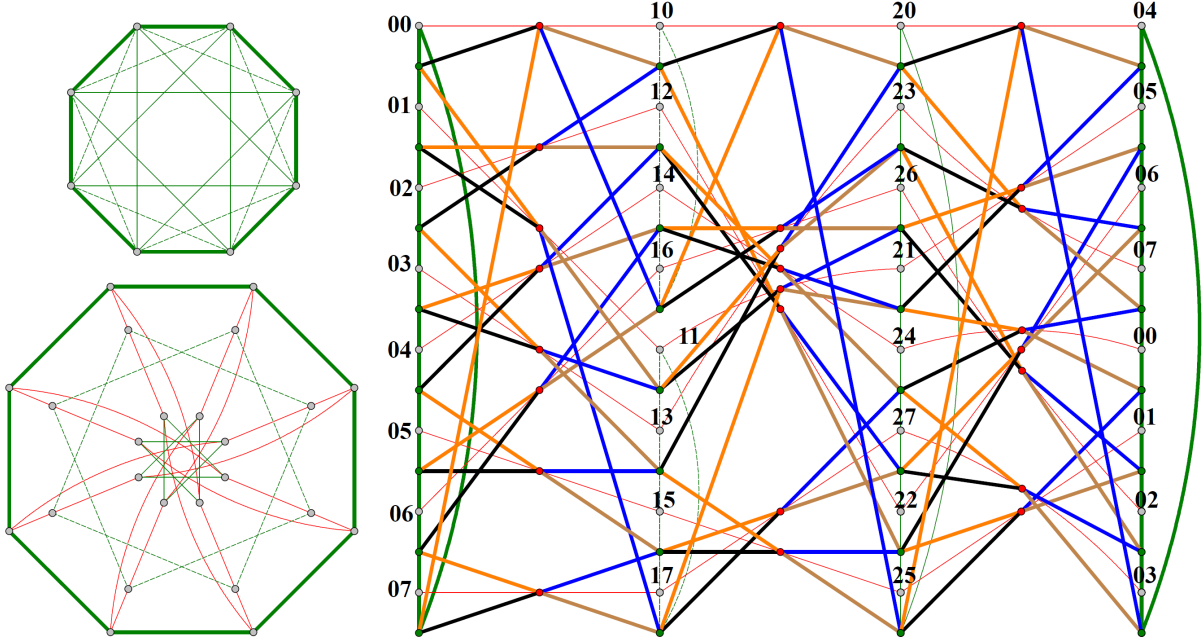


Figure 12: Tight factorization of $\mathbb{P}(\text{MBr}(3, \{F_1^8, F_2^8, F_3^8\}))$, based on 2-factors of K_8 .

$(0_1^0[a]_1^0 1[b]_0 0_2^1[c]_0^2 1[d])$	$(1_2^0[c]_1^0 2[d] 1_4^2[a]_2 2[b])$	$(2_3^0[a]_0^2 3[b] 2_6^3[c]_2 3[d])$
$(0_2^1[a]_1^0 2[b] 0_3^2[c]_0^2 2[d])$	$(1_3^1[c]_1^0 3[d] 1_5^3[a]_2 3[b])$	$(2_4^1[a]_0^2 4[b] 2_0^4[c]_2 4[d])$
$(0_3^2[a]_1^0 3[b] 0_4^3[c]_0^2 3[d])$	$(1_4^2[c]_1^0 4[d] 1_6^4[a]_2 4[b])$	$(2_5^2[a]_0^2 5[b] 2_1^5[c]_2 5[d])$
$(0_4^3[a]_1^0 4[b] 0_5^4[c]_0^2 4[d])$	$(1_5^3[c]_1^0 5[d] 1_0^5[a]_2 5[b])$	$(2_6^3[a]_0^2 6[b] 2_2^6[c]_2 6[d])$
$(0_5^4[a]_1^0 5[b] 0_6^5[c]_0^2 5[d])$	$(1_6^4[c]_1^0 6[d] 1_1^6[a]_2 6[b])$	$(2_0^4[a]_0^2 0[b] 2_3^4[c]_2 0[d])$
$(0_6^5[a]_1^0 6[b] 0_0^6[c]_0^2 6[d])$	$(1_0^5[c]_1^0 0[d] 1_2^0[a]_2 0[b])$	$(2_1^5[a]_0^2 1[b] 2_4^1[c]_2 1[d])$
$(0_0^6[a]_1^0 0[b] 0_1^0[c]_0^2 0[d])$	$(1_1^6[c]_1^0 1[d] 1_3^1[a]_2 1[b])$	$(2_2^6[a]_0^2 2[b] 2_5^2[c]_2 2[d])$
$(0_1^0[a]_1^0 1[b] 0_5^1[c]_0^2 5[d])$	$(1_2^1[c]_1^0 2[d] 1_0^2[a]_2 0[b])$	$(2_3^2[a]_0^2 3[b] 2_1^3[c]_2 1[d])$
$(0_5^1[a]_1^0 5[b] 0_2^2[c]_0^2 2[d])$	$(1_0^2[c]_1^0 0[d] 1_3^0[a]_2 2[b])$	$(2_1^3[a]_0^2 1[b] 2_4^1[c]_2 4[d])$
$(0_2^2[a]_1^0 2[b] 0_4^2[c]_0^2 4[d])$	$(1_3^0[c]_1^0 3[d] 1_5^3[a]_2 5[b])$	$(2_4^1[a]_0^2 4[b] 2_0^4[c]_2 0[d])$
$(0_4^2[a]_1^0 4[b] 0_3^3[c]_0^2 3[d])$	$(1_5^3[c]_1^0 5[d] 1_4^5[a]_2 4[b])$	$(2_0^4[a]_0^2 0[b] 2_5^4[c]_2 5[d])$
$(0_3^3[a]_1^0 3[b] 0_6^3[c]_0^2 6[d])$	$(1_4^5[c]_1^0 4[d] 1_6^4[a]_2 6[b])$	$(2_5^4[a]_0^2 5[b] 2_6^5[c]_2 6[d])$
$(0_6^3[a]_1^0 6[b] 0_0^6[c]_0^2 0[d])$	$(1_6^4[c]_1^0 6[d] 1_1^6[a]_2 1[b])$	$(2_6^5[a]_0^2 6[b] 2_2^6[c]_2 2[d])$
$(0_0^6[a]_1^0 0[b] 0_1^0[c]_0^2 1[d])$	$(1_1^6[c]_1^0 1[d] 1_2^1[a]_2 2[b])$	$(2_2^6[a]_0^2 2[b] 2_3^2[c]_2 3[d])$
$(0_1^0[a]_1^0 1[b] 0_6^1[c]_0^2 6[d])$	$(1_3^1[c]_1^0 3[d] 1_1^3[a]_2 1[b])$	$(2_0^2[a]_0^2 2[b] 2_1^2[c]_2 1[d])$
$(0_6^1[a]_1^0 6[b] 0_0^6[c]_0^2 6[d])$	$(1_1^3[c]_1^0 1[d] 1_5^1[a]_2 6[b])$	$(2_1^2[a]_0^2 1[b] 2_4^1[c]_2 4[d])$
$(0_0^6[a]_1^0 0[b] 0_1^0[c]_0^2 0[d])$	$(1_5^1[c]_1^0 5[d] 1_0^5[a]_2 0[b])$	$(2_4^1[a]_0^2 4[b] 2_0^4[c]_2 0[d])$
$(0_3^0[a]_1^0 3[b] 0_4^3[c]_0^2 3[d])$	$(1_0^5[c]_1^0 0[d] 1_3^0[a]_2 3[b])$	$(2_0^4[a]_0^2 0[b] 2_0^4[c]_2 2[d])$
$(0_4^3[a]_1^0 4[b] 0_5^4[c]_0^2 4[d])$	$(1_2^4[c]_1^0 4[d] 1_6^4[a]_2 6[b])$	$(2_3^5[a]_0^2 5[b] 2_6^5[c]_2 6[d])$
$(0_5^4[a]_1^0 5[b] 0_2^5[c]_0^2 5[d])$	$(1_6^4[c]_1^0 6[d] 1_2^6[a]_2 2[b])$	$(2_6^5[a]_0^2 6[b] 2_3^6[c]_2 3[d])$
$(0_2^5[a]_1^0 2[b] 0_3^2[c]_0^2 2[d])$	$(1_2^6[c]_1^0 2[d] 1_4^2[a]_2 4[b])$	$(2_3^6[a]_0^2 2[b] 2_5^3[c]_2 5[d])$

Table 6: Code representations of F_1^7 , F_2^7 and F_3^7 .

$(0_1^0[a]_1^0 1[b]_2^0 1[c]_0^3 1[d])$	$(1_2^0[a]_2^1 2[b]_4^2 1[c]_0^2 2[d])$	$(2_3^0[a]_3^2 3[b]_6^3 2[c]_2^1 3[d])$	$(3_4^0[a]_4^3 4[b]_8^4 3[c]_3^2 4[d])$
$(0_2^1[a]_1^0 2[b]_3^0 2[c]_0^3 2[d])$	$(1_3^1[a]_2^1 3[b]_5^3 1[c]_0^3 3[d])$	$(2_4^1[a]_3^2 4[b]_7^4 2[c]_2^1 4[d])$	$(3_5^1[a]_0^3 5[b]_6^5 3[c]_3^2 5[d])$
$(0_3^2[a]_1^0 3[b]_4^0 3[c]_0^3 3[d])$	$(1_4^2[a]_2^1 4[b]_6^4 1[c]_1^0 4[d])$	$(2_5^2[a]_3^2 5[b]_8^5 2[c]_2^1 5[d])$	$(3_6^2[a]_0^3 6[b]_5^6 3[c]_3^2 6[d])$
$(0_4^3[a]_1^0 4[b]_5^0 4[c]_0^3 4[d])$	$(1_5^3[a]_2^1 5[b]_7^5 1[c]_1^0 5[d])$	$(2_6^3[a]_3^2 6[b]_9^6 2[c]_2^1 6[d])$	$(3_7^3[a]_0^3 7[b]_6^7 3[c]_3^2 7[d])$
$(0_5^4[a]_1^0 5[b]_6^0 5[c]_0^3 5[d])$	$(1_6^4[a]_2^1 6[b]_8^6 1[c]_1^0 6[d])$	$(2_7^4[a]_3^2 7[b]_{10}^7 2[c]_2^1 7[d])$	$(3_8^4[a]_0^3 8[b]_7^8 3[c]_3^2 8[d])$
$(0_6^5[a]_1^0 6[b]_7^0 6[c]_0^3 6[d])$	$(1_7^5[a]_2^1 7[b]_{11}^7 1[c]_1^0 7[d])$	$(2_8^5[a]_3^2 8[b]_{12}^8 2[c]_2^1 8[d])$	$(3_9^5[a]_0^3 9[b]_8^9 3[c]_3^2 9[d])$
$(0_7^6[a]_1^0 7[b]_8^0 7[c]_0^3 7[d])$	$(1_8^6[a]_2^1 8[b]_{12}^8 1[c]_1^0 8[d])$	$(2_9^6[a]_3^2 9[b]_{13}^9 2[c]_2^1 9[d])$	$(3_{10}^6[a]_0^3 10[b]_9^{10} 3[c]_3^2 10[d])$
$(0_8^7[a]_1^0 8[b]_9^0 8[c]_0^3 8[d])$	$(1_9^7[a]_2^1 9[b]_{13}^9 1[c]_1^0 9[d])$	$(2_{10}^7[a]_3^2 10[b]_{14}^{10} 2[c]_2^1 10[d])$	$(3_{11}^7[a]_0^3 11[b]_{10}^{11} 3[c]_3^2 11[d])$
$(0_9^8[a]_1^0 9[b]_{10}^0 9[c]_0^3 9[d])$	$(1_{10}^8[a]_2^1 10[b]_{14}^{10} 1[c]_1^0 10[d])$	$(2_{11}^8[a]_3^2 11[b]_{15}^{11} 2[c]_2^1 11[d])$	$(3_{12}^8[a]_0^3 12[b]_{11}^{12} 3[c]_3^2 12[d])$

Table 7: Tight factorization of $\mathbb{P}(4, F^9)$.

to the edges $(i_j^{j+r^i}, i^{+1}j)$, $(i_j^{j+r^i}, i^{+1}(j+r^i))$, $((i+1)_j^{j+r^i}, i^{+1}(j+r^i))$ and $((i+1)_j^{j+r^i}, i^{+1}j)$, respectively, yields a tight factorization of $\mathbb{P}(\text{Br}(k, n; r))$.

A code representation of the tight factorization in Fig. 10(a) is given in Table 5, where each green edge $\{ij, i(j+r^i)\}$ in $\text{Br}(k, n; r)$ yields a green vertex $i_j^{j+r^i}$ in $\mathbb{P}(\text{Br}(k, n; r))$, each red edge $\{ij, (i+1)j\}$ in $\text{Br}(k, n; r)$ yields a red vertex $i^{+1}j$ in $\mathbb{P}(\text{Br}(k, n; r))$, and the color of an edge between a green vertex and a red vertex is indicated between brackets: $[a]$ for orange, $[b]$ for black, $[c]$ for hazel and $[d]$ for blue.

Remark 26. Generalizing Remark 25 to get other egc girth-tight graphs, we consider a 2-factorization $F^n = \{F_1^n, F_2^n, \dots, F_{k-1}^n\}$ of the complete graph K_n , for odd $n = 2k + 1 > 6$ and use it to define the *barrel* $\text{Br}(k, F^n)$, with

- (i) $\mathbb{Z}_k \times \mathbb{Z}_n$ as vertex set and
- (ii) edges forming precisely red cycles $((0, i), (1, i), \dots, (k-1, i))$, where $i \in \mathbb{Z}_n$, and green subgraphs $\{j\} \times F_j^n$, where $j \in \mathbb{Z}_k$.

Fig. 11 contains representations of $\mathbb{P}(\text{Br}(3, F^7))$ for three distinct 2-factorizations F^7 of K_7 , with tight factorizations represented as in Fig. 10, with green cycles so that each vertex $(i, 0) = i0$ appears just once (not twice, as in Fig. 10(a–b)). In the three cases, F_1^7 , F_2^7 and F_3^7 , green edges are traced thick, thin and dashed, respectively. To the left of these representations, the corresponding green subgraphs are shown. Code representations of these three tight factorizations can be found in Table 6, following the conventions of Table 5. (A different 1-factorization of K_7 that may be used with the same purpose is for example $((0, 1, 2, 3, 4, 5, 6), (0, 3, 5, 1, 6, 2, 4), (0, 2, 5)(1, 3, 6, 4))$.

In the same way, by considering the 2-factorization given in K_9 seen as the Cayley graph $C_9(1, 2, 3, 4)$ with F^9 formed by the 2-factors $F_1^9, F_2^9, F_3^9, F_4^9$ generated by the respective colors 1, 2, 3, 4, namely Hamilton cycles F_1^9, F_2^9, F_4^9 but $F_3^9 = 3K_3$, we get a tight factorization of $\mathbb{P}(4, F^9)$. This is encoded in Table 7 in a similar fashion to that of Tables 4–5.

If $n = 2k$ is even, a similar generalization takes a 2-factorization $F^n = \{F_1^n, F_2^n, \dots, F_{k-2}^n\}$ of $K_n - \{i(i+k); i = 0, \dots, k-1\}$ and uses the 1-factor $\{i(i+k); i = 0, \dots, k-1\}$ to get

a generalized *mutant barrel* $\text{MBr}(k-1, F^n)$ in a likewise fashion to that of item (b) in Remark 25 but modified now via F^n , namely with

- (i') $\mathbb{Z}_{k-1} \times \mathbb{Z}_n$ as vertex set and
- (ii') edges forming precisely red cycles $((0, i), (1, i), \dots, (k-1, i), (0, i + \frac{n}{2}), (1, i + \frac{n}{2}), \dots, (k-1, i + \frac{n}{2}))$, where $i \in \mathbb{Z}_n$, and green subgraphs $\{j\} \times F_j^n$, where $j \in \mathbb{Z}_k$.

Fig. 12 represents a tight factorization of $\mathbb{P}(\text{MBr}(3, F^8))$, where $F^8 = \{F_1^8, F_2^8, F_3^8\}$, represented on the upper left of the figure, is such a 2-factorization, with F_1^8 and F_3^8 as in Fig. 10, and $F_2^8 = (0, 2, 4, 6)(1, 3, 5, 7)$, via corresponding thick, thin and dashed, green edge tracing. On the lower left, a representation of the red-green graph $\text{MBr}(3, F^8)$ is found.

We can further extend these notions of barrel and mutant barrel by taking a cycle $G^n = (G_1^n, G_2^n, \dots, G_\ell^n)$ of copies of the 2-factors of F^n , where $G_i^n \in F^n$ but with no two contiguous G_i^n and $G_{i+1}^n \pmod n$ being the same element of F^n . Here, $\ell \geq 3$. This defines a barrel $\text{Br}(\ell, G^n)$ or mutant barrel $\text{MBr}(\ell, G^n)$ (n even in this case) and establishes the following.

Theorem 27. *The barrels and mutant barrels obtained in Remark 26 produce corresponding egc graphs $\mathbb{P}(\text{Br}(\ell, G^n))$ and $\mathbb{P}(\text{MBr}(\ell, G^n))$.*

Proof. The zigzagging orange-black and hazel-blue cycles between each pair of contiguous green-vertex and red-vertex columns in the graphs of Fig. 10–12 are as in Lemma 9. \square

6 EgC girth-g-regular graphs, g larger than 4

Theorem 28. *We have the following:*

- (a) *the 32-vertex Armanios-Wells graph AW [1] [2, p. 266] is an egC $(12)^5$ -graphs;*
- (b) *the 36-vertex Sylvester graph Syl [2, p. 223] is a 8^5 -graph, but is not egC.*

Proof. (a) The center of Fig. 13 represents AW colored as claimed. The vertices of AW are denoted Xi ($X \in \{A, B, C, D\}; i \in \mathbb{Z}_8$). An edge-color assignment for AW is generated mod 4 or $(\text{mod } \mathbb{Z}_4)$, where $\mathbb{Z}_4 = \{0, 2, 4, 6\} \subset \mathbb{Z}_8$ is a subgroup and an ideal of \mathbb{Z}_8 , as follows:

<i>Red</i>	1	$(A0, C7)$	$(A1, C2)$	$(B0, D1)$	$(B1, D2)$	(4)
<i>Black</i>	2	$(A0, C1)$	$(A1, C0)$	$(B0, B3)$	$(D0, D1)$	
<i>Blue</i>	3	$(A0, D6)$	$(A1, B4)$	$(B1, C6)$	$(C1, D3)$	
<i>Hazel</i>	4	$(A0, B3)$	$(A1, D7)$	$(B0, C5)$	$(C0, D2)$	
<i>Green</i>	5	$(A0, C6)$	$(A1, C7)$	$(B0, B5)$	$(D1, D2)$	

where indices are taken $(\text{mod } 8)$, so colored-edge orbits $(\text{mod } 4)$ are either of the form

$$\{(X0, Yi), (X2, Y(i+2)), (X4, Y(i+4)), (X6, Y(i+6))\} \text{ or of the form: } \\ \{(X1, Yj), (X3, Y(j+2)), (X5, Y(j+4)), (X7, Y(j+6))\}$$

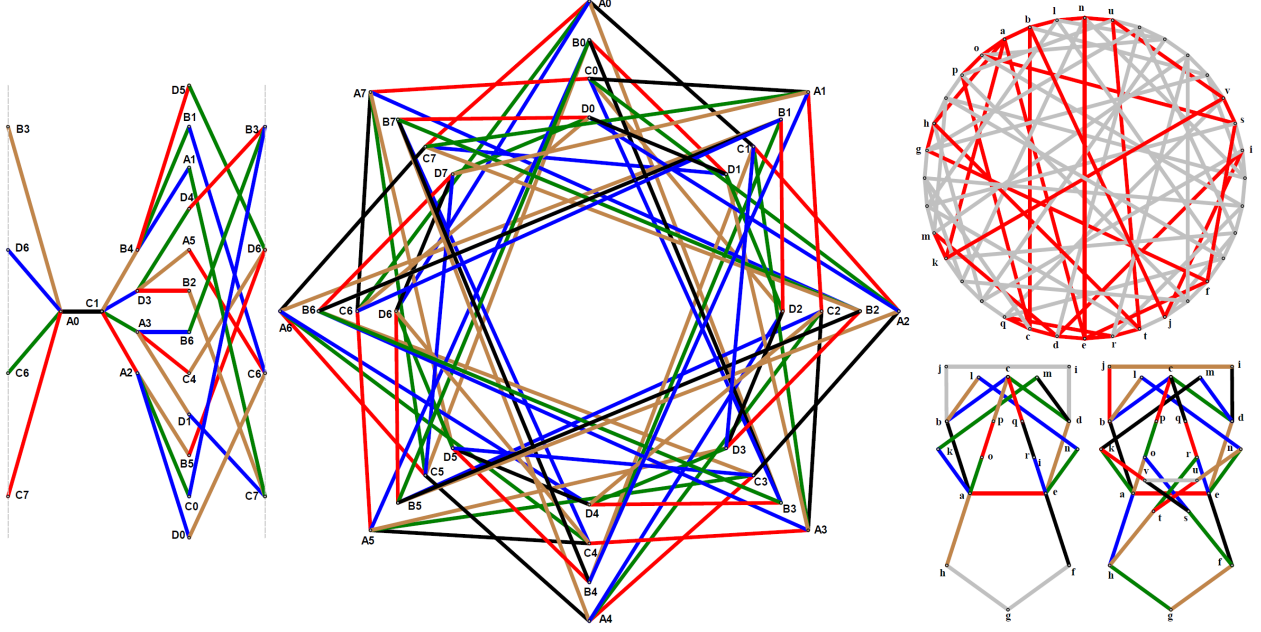


Figure 13: The egc Armanios-Wells $(12)^5$ -graph and the non-egc Sylvester 8^4 -graph.

with $X, Y \in \{A, B, C, D\}$, $i, j \in \mathbb{Z}_8$ and addition taken (mod 8). The left of Fig. 13 contains the subgraph of AW spanned by the twelve 5-cycles through the black edge (A_0, C_1) (where the two dashed lines must be identified), showing the disposition of twelve 5-cycles around an edge of AW. Moreover, the four black edges in the second line of (4) represent forty-eight tightly colored 5-cycles, (twelve passing through each black edge, corresponding to the $\frac{5!}{2 \times 5} = 12$ existing color cycles

$$(23451), (23541), (24351), (24531), (25341), (25431), \\ (24513), (25413), (25134), (24135), (23514), (25143))$$

and each such cycle yields an orbit of four such 5-cycles. Since each edge of AW passes through twelve 5-cycles of AW and $|E(AW)| = 80$, we count 80×12 5-cycles in AW with repetitions. Each 5-cycle in this count is repeated five times, so the number of 5-cycles in AW is $(80 \times 12)/5 = 16 \times 12$. Thus, the number of orbits of tightly-colored 5-cycles is 48 and we obtain a tight coloring of AW.

(b) The upper right of Fig. 13 represents Syl with the following 5-cycles:

$$C_0 = (abcde) \quad C_1 = (aefgh) \quad C_2 = (abcgh) \quad C_3 = (cdefg) \quad C_4 = (bcdij) \quad C_5 = (hidea) \\ C_6 = (hijba) \quad C_7 = (cghid) \quad C_8 = (akmde) \quad C_9 = (ablne) \quad C_{10} = (abcpo) \\ C_{11} = (cderq) \quad C_{12} = (aefso) \quad C_{13} = (eahtr) \quad C_{14} = (aksvo) \quad C_{15} = (enutr).$$

The union of C_0, C_1, C_4, C_8, C_9 yields the red subgraph. Coloring tightly $C_0, C_8, C_9, C_{10}, C_{11}$ with $\text{color}(ab) = \text{color}(ef)$ and $\text{color}(ah) = \text{color}(de)$ makes impossible continuing coloring tightly C_4 , see Syl as shown in the upper right of Fig. 13. Otherwise, in the lower right of Fig. 13 a forced tight coloring of $C_0, \dots, C_{12}, C_{14}$ and C_{15} is shown in two representations of

the subgraph of Syl induced by these 5-cycles. That leaves C_{13} obstructing a tight-coloring. Thus, Syl is not egc. \square

Subsequently, an egc $4^3 0^2$ -graph Γ is presented by means of a construction that generalizes the barrel constructions used in Section 5, as follows. See the top of Fig. 14, where fourteen vertical copies of the Petersen graph Pet are presented in parallel at equal distances from left to right and numbered from 0 to 13 in \mathbb{Z}_{14} . The vertices of the j -th copy Pet ^{j} of Pet are denoted $v_1^j, v_2^j, \dots, v_{10}^j$ from top to bottom and are joined horizontally by cycles of the Cayley graph of \mathbb{Z}_{14} with generator set $\{1, 3, 5\}$, namely the cycles

$$\begin{aligned} & (v_i^0, v_i^1, v_i^2, v_i^3, v_i^4, v_i^5, v_i^6, v_i^7, v_i^8, v_i^9, v_i^{10}, v_i^{11}, v_i^{12}, v_i^{13}), & \text{for } i = 1, 5, 7, 9; \\ & (v_i^0, v_i^3, v_i^6, v_i^9, v_i^{12}, v_i^1, v_i^4, v_i^7, v_i^{10}, v_i^{13}, v_i^2, v_i^5, v_i^8, v_i^{11}), & \text{for } i = 2, 3, 4; \\ & (v_i^0, v_i^5, v_i^{10}, v_i^1, v_i^6, v_i^{11}, v_i^2, v_i^7, v_i^{12}, v_i^3, v_i^8, v_i^{13}, v_i^4, v_i^9), & \text{for } i = 6, 8, 10. \end{aligned} \quad (5)$$

Theorem 29. *There exists an egc $4^3 0^2$ -graph Γ of order $140 \times k$, for every $0 < k \in \mathbb{Z}$, representing all color-cycle permutations, $14k$ times each.*

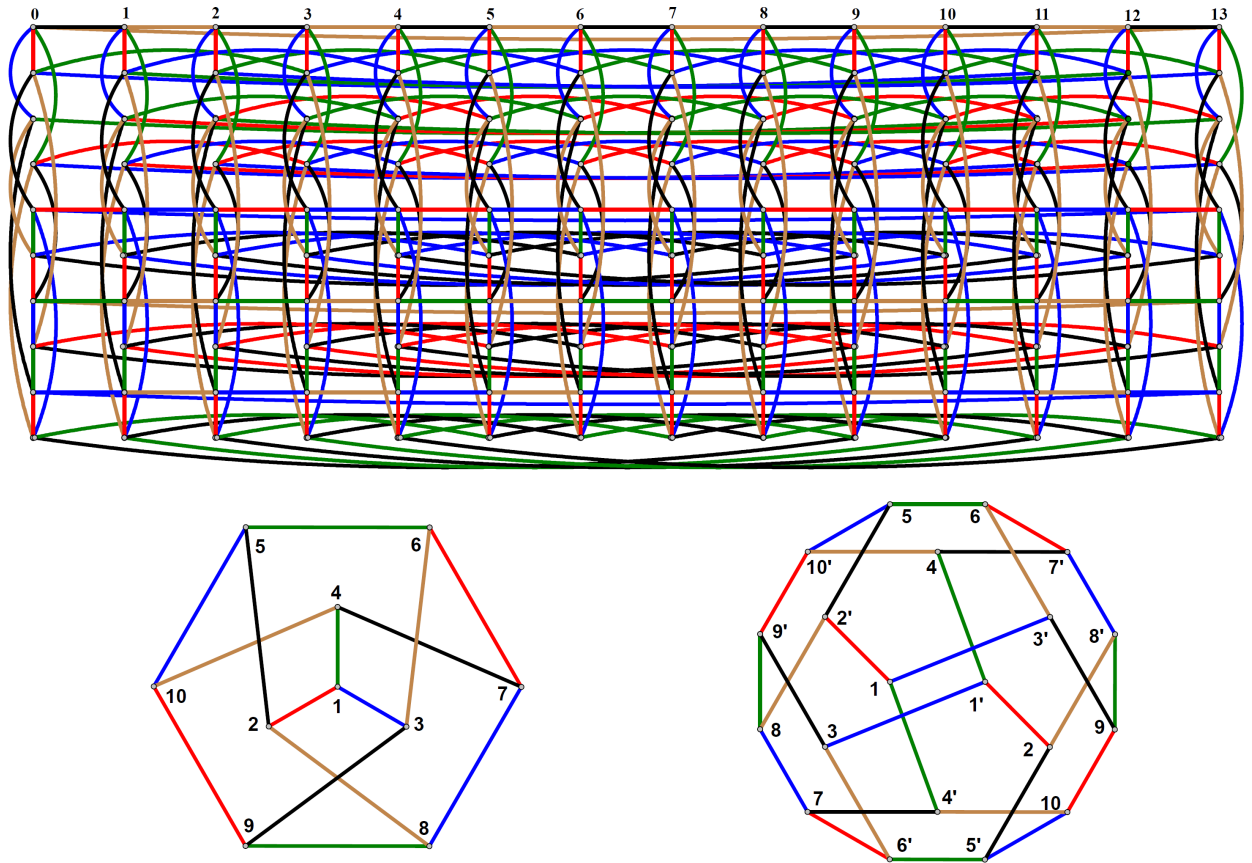


Figure 14: Egc $4^3 0^2$ -graph on 140 vertices; Petersen and dodecahedral graphs.

Proof. We assert that an egc $4^3 0^2$ -graph as in the statement contains $14k$ disjoint copies of Pet . We consider the case represented in the top of Fig. 14 for $k = 1$ and leave the details of the general case to the reader. Notice the 6-cycle $(v_5^j, v_6^j, v_7^j, v_8^j, v_9^j, v_{10}^j)$ in Pet^j , with its three pairs of opposite vertices $\{v_5^j, v_8^j\}$, $\{v_6^j, v_9^j\}$, $\{v_7^j, v_{10}^j\}$ joined respectively to the neighbors v_2^j, v_3^j, v_4^j of the top vertex v_1^j , for $j \in \mathbb{Z}_{14}$. A representation of the common proper coloring of the graphs Pet^j is in the lower-left part of Fig. 14, where the vertices v_i^j , for $i = 1, \dots, 10$ and $j \in \mathbb{Z}_{14}$, are simply denoted i . This figure shows the twelve 5-cycles of Pet as color cycles, with red, black, blue, hazel and green taken respectively as 1, 2, 3, 4 and 5. This gives the one-to-one correspondence, call it η , from the 5-cycles of Pet onto their color 5-cycles in the top part of Table 8.

There are exactly twelve color 5-cycles; they are the targets η . They are obtained from the $5! = 120$ permutations on five objects as the twelve orbits of the dihedral group D_{10} generated both by translations (mod 5) and by reflections of the 5-tuples on $\{1, 2, 3, 4, 5\}$. The edges of Γ not in $\cup_{j=0}^{13} Pet^j$ occur between different copies Pet^j of Pet ; these are colored as shown in the bottom part of Table 8. This insures the statement for $k = 1$, since the twelve vertical copies Pet^j of Pet are the only source of the color cycles. The extension of this for any $0 < k \in \mathbb{Z}$ is immediate. \square

The dodecahedral graph Dod with vertex set $\{u_i, w_i | i = 1, 2, \dots, 10\}$ and edge set formed by an edge pair $\{(u_i, w_{i'}), (u_{i'}, w_i)\}$ for each $(v_i, v_{i'}) \in (E(Pet) \setminus \{(v_5, v_6), (v_7, v_8), (v_9, v_{10})\})$ and an edge pair $\{(u_i, u_{i+1}), (w_i, w_{i+1})\}$ for each $i \in \{5, 7, 9\}$, is represented in the lower-right of Fig. 14, where u_i and w_i (that we will refer to as antipodal vertices) are respectively indicated by i and i' , for $i = 1, \dots, 10$. Dod is a 2-covering graph of Pet via the graph map $\phi : Dod \rightarrow Pet$ such that $\phi^{-1}(\{v_i\}) = \{u_i, w_i\}$.

Theorem 30. *There exists an egc $2^3 0^2$ -graph Γ of order $140 \times k$, for every $0 < k \in \mathbb{Z}$.*

Proof. We consider the case $k = 1$ and leave the details of the general case to the reader. We take seven vertical copies of Dod presented in parallel at equal distances from left to right and numbered from 0 to 6 in \mathbb{Z}_7 . The vertices of the j -th copy Dod^j of Dod are denoted u_i^j and w_i^j , for $i = 1, \dots, 10$ and are joined by the additional cycles

$$\begin{aligned} & (u_i^0, u_i^1, u_i^2, u_i^3, u_i^4, u_i^5, u_i^6, w_i^0, w_i^1, w_i^2, w_i^3, w_i^4, w_i^5, w_i^6), & \text{for } i = 1, 5, 7, 9; \\ & (u_i^0, u_i^3, u_i^6, u_i^2, u_i^5, u_i^1, u_i^4, w_i^0, w_i^3, w_i^6, w_i^2, w_i^5, w_i^1, w_i^4), & \text{for } i = 6, 8, 10; \\ & (u_i^0, u_i^5, u_i^3, u_i^1, u_i^6, u_i^4, u_i^2, w_i^0, w_i^5, w_i^3, w_i^1, w_i^6, w_i^4, w_i^2), & \text{for } i = 2, 3, 4. \end{aligned} \tag{6}$$

so that each such additional cycle passes through two antipodal vertices of each copy Dod^j . Notice the change of the order of the indices $i \in \{1, \dots, 10\}$ in the assignment of the additional cycles in display (6) with respect to the one in display (5). This is done to avoid the formation of 5-cycles not entirely contained in the copies Dod^j ($j \in \mathbb{Z}_7$). Since Dod has girth 5 and signature $2^3 = 222$, the graph Γ given by the union of the seven copies Dod^j and the just presented additional cycles is a $2^3 0^2$ -graph. By coloring the edges of the additional cycles of Γ via the same color pattern as in Theorem 29, it is seen that Γ is egc. \square

The truncated-icosahedral graph TI is the graph of the truncated icosahedron. This is obtained from the icosahedral graph, i.e. the line graph $Ico = L(Dod)$ of Dod , by replacing

(1, 2, 5, 10, 4) → (1, 2, 3, 4, 5)	(3, 6, 7, 8, 9) → (4, 1, 3, 5, 2)
(4, 1, 2, 8, 7) → (5, 1, 4, 3, 2)	(10, 9, 3, 6, 5) → (1, 2, 4, 5, 3)
(1, 2, 5, 6, 3) → (1, 2, 5, 4, 3)	(4, 7, 8, 9, 10) → (2, 3, 5, 1, 4)
(2, 5, 10, 9, 8) → (2, 3, 1, 5, 4)	(1, 3, 6, 7, 4) → (3, 4, 1, 2, 5)
(5, 10, 4, 7, 6) → (3, 4, 2, 1, 5)	(2, 8, 9, 3, 1) → (4, 5, 2, 3, 1)
(10, 4, 1, 3, 9) → (4, 5, 3, 2, 1)	(5, 6, 7, 8, 2) → (5, 1, 3, 4, 2)

(v_1^j, v_1^{j+1}) has color 2, if $j \equiv 0 \pmod{2}$ and 4, if $j \equiv 1 \pmod{2}$
(v_5^j, v_5^{j+1}) has color 1, if $j \equiv 0 \pmod{2}$ and 3, if $j \equiv 1 \pmod{2}$
(v_7^j, v_7^{j+1}) has color 5, if $j \equiv 0 \pmod{2}$ and 4, if $j \equiv 1 \pmod{2}$
(v_9^j, v_9^{j+1}) has color 3, if $j \equiv 0 \pmod{2}$ and 4, if $j \equiv 1 \pmod{2}$
(v_2^j, v_2^{j+3}) has color 5, if $j \equiv 0 \pmod{2}$ and 3, if $j \equiv 1 \pmod{2}$
(v_3^j, v_3^{j+3}) has color 1, if $j \equiv 0 \pmod{2}$ and 5, if $j \equiv 1 \pmod{2}$
(v_4^j, v_4^{j+3}) has color 1, if $j \equiv 0 \pmod{2}$ and 3, if $j \equiv 1 \pmod{2}$
(v_6^j, v_6^{j+5}) has color 3, if $j \equiv 0 \pmod{2}$ and 2, if $j \equiv 1 \pmod{2}$
(v_8^j, v_8^{j+5}) has color 1, if $j \equiv 0 \pmod{2}$ and 2, if $j \equiv 1 \pmod{2}$
(v_{10}^j, v_{10}^{j+5}) has color 5, if $j \equiv 0 \pmod{2}$ and 2, if $j \equiv 1 \pmod{2}$

Table 8: Color assignment of the $4^3 0^2$ -graph Γ in Theorem 29

each vertex v of Ico by a copy $C_5^{TI}(v)$ of its open neighborhood $N_{Ico}(v)$, considering all such copies $C_5^{TI}(v)$ pairwise disjoint, and replacing each edge (u, v) of Ico by an edge from the vertex corresponding to u in $C_5^{TI}(v)$ to the vertex corresponding to v in $C_5^{TI}(u)$. Note TI has sixty vertices, ninety edges, twelve 5-cycles, twenty 6-cycles and signature $1^2 0 = 110$.

Theorem 31. *There exists an egc 10^4 -graph on $840k$ vertices, for each integer $k > 0$.*

Proof. By means of a barrel-type construction as in Fig. 14, one can combine $14k$ copies of TI and the Cayley graph of \mathbb{Z}_{14} with generator set $\{1, 3, 5\}$ to get an egc graph as claimed. \square

Remark 32. The point graph of the generalized hexagon $GH(1, 5)$ [2, p. 204], the point graph of the Van Lint–Schrijver partial geometry [2, p. 307] and the odd graph [2, p. 259] on eleven points are distance-regular with intersection arrays $\{6, 5, 5; 1, 1, 6\}$, $\{6, 5, 5, 4; 1, 1, 2, 6\}$ and $\{6, 5, 5, 4, 4; 1, 1, 2, 2, 3\}$, respectively. If their chromatic number were 6, they would be $(125)^6$ -, $(25)^6$ - and $(25)^6$ -graphs, respectively, but it is known that none of them is egc.

7 Hamilton cycles and hamiltonian decomposability

Some feasible applications of egc graphs occur when the unions of pairs of composing 1-factors are Hamilton cycles, possibly attaining hamiltonian decomposability in the even-degree case. This offers a potential benefit to the applications drawn in Section 1, if an optimization/decision-making problem requires alternate inspections covering all nodes of the involved system, when the alternacy of two colors is required.

In Fig. 1, the cases (h–j) and their triangle-replaced graphs (m–o) as well as the case (u), and the 3-colored dodecahedral graph Dod that has the case (u) as its triangle replaced graph, have the unions of any two of their 1-factors forming a Hamilton cycle, while the cases (k), (p) and (v) have those unions as disjoint pairs of two cycles of equal length. In particular, the 3-cube graph Q_3 that admits just two tight factorizations, has one of them creating Hamilton cycle (case (l) via green and either red or blue edges, but not red and blue edges). The triangle-replaced graph, $\nabla(Q_3)$, has corresponding tight factorizations in cases (p–q) with similar differing properties as those of cases (k–l). Preceding Theorem 4, similar comments are made for $\nabla(\Gamma')$, where Γ' is Dod or the Coxeter graph Cox . Recall the union of two 1-factors of Dod is hamiltonian while the union of two 1-factors of Cox is not.

$s = 1$	5	7	9	11	13	15	$s = 3$	5	7	9	$s = 5$	5	7	9
$r = 6$	113						$r = 6$	131						
$r = 8$	211	114					$r = 8$	114	211					
$r = 10$	111	111	511				$r = 10$	111	511	111	$r = 10$	555	151	151
$r = 12$	213	312	112	116			$r = 12$	132	233	336	$r = 12$	611	611	211
$r = 14$	111	111	111	111	117		$r = 14$	141	111	111	$r = 14$	711	111	117
$r = 16$	211	114	114	112	211	118	$r = 16$	411	112	112	$r = 16$	811	211	211
$r = 18$	113	311	111	311	311	111	$r = 18$	131	131	333	$r = 18$	911	111	111
$r = 20$	211	112	215	215	112	112	$r = 20$	211	512	112	$r = 20$	$a51$	251	251
$r = 22$	111	111	111	111	111	111	$r = 22$	111	111	111	$r = 22$	$b11$	111	111
$r = 24$	213	314	411	611	611	114	$r = 24$	133	231	336	$r = 24$	$c11$	211	211
$r = 26$	111	111	111	111	111	111	$r = 26$	111	111	111	$r = 26$	$d11$	111	111
$r = 28$	211	112	211	211	217	711	$r = 28$	112	211	112	$r = 28$	$e11$	211	217
$r = 30$	113	311	115	115	111	111	$r = 30$	132	135	333	$r = 30$	$f11$	151	111

Table 9: Various cases of Theorem 10 item 3(e).

In Fig. 2(d), the three color partitions of Q_4 , namely (12)(34), (13)(24) and (14)(23), yield 2-factorizations with 2-factors formed each by two cycles of equal length $\frac{1}{2}|V(Q_4)| = 8$. We denote this facts by writing $Q_4(2, 2, 2)$. In a likewise fashion, we can denote toroidal items in Fig. 2 as follows: (e) $\{4, 4\}_{12,2}^4(1, 4, 3)$, formed by 2-factorizations with 2-factors of one, three and four cycles of equal lengths 24, 6 and 8, respectively. Similarly: (f) $\{4, 4\}_{10,2}^4(1, 2, 1)$; (g) $\{4, 4\}_{6,3}^3(3, 3, 3)$; (h) $\{4, 4\}_{20,1}^0(2, 1, 1)$; (i) $\{4, 4\}_{28,1}^0(1, 1, 2)$; and (j) $\{4, 4\}_{22,1}^5(1, 2, 1)$.

Table 9 lists various cases of Theorem 10 item 3(e), indicating without parentheses or commas the triples abc corresponding to the numbers a , b and c of cycles (of equal length in each case) of the respective 2-factors (12), (13) and (14).

Remark 33. For the toroidal cases in Theorem 10 item 3 depicted as in Fig. 2(f,g,h,j), assume that the 2-factors (12) and (14) complete 2-factorizations composed by 1-zigzagging cycles of equal length (i.e., composed by alternating horizontal and vertical edges) and that the 2-factors (13) and (24) are composed by vertical and horizontal edges, respectively. This way, while vertical edges form $\gcd(r, s)$ cycles of equal length, horizontal edges form t cycles

of not necessarily the same length, so the notation in the previous paragraph cannot be carried out for example for item 3(e) because $\gcd(r, s) \neq t$. So we modify that notation for such cases by simply writing $\{4, 4\}_{r,t}^s(a, b, c)$, that we call the *star notation* [9].

Theorem 34. *In the star notation of Remark 33, each applicable toroidal case $\Gamma = \{4, 4\}_{r,t}^s$ as in Theorem 10 is expressible as: $\{4, 4\}_{r,t}^s(\frac{1}{2} \gcd(r, |t - s|), \gcd(r, s), \frac{1}{2} \gcd(r, t + s))$.*

Proof. We prove the statement for the toroidal cases of Theorem 10 with two colors on horizontal cycles and the other two on vertical cycles, for the factorization $\{F_{12}, F_{34}\}$, and leave the rest to the reader. Consider the straight upper-right-to-lower-left line L_1 from the upper-right vertex $(0, 0)$ in the cutout Φ (Remark 5) of $\mathbb{Z}_r \times \mathbb{Z}_t$ passing through $(0, r - t + s)$ in the lower border of Φ and formed by the diagonals of $\frac{rt}{2 \gcd(r, |t - s|)}$ squares representing 4-cycles of Γ . L_1 determines two 1-zigzagging cycles C_1^0, C_1^1 through $(0, 0)$ in F_{12}, F_{34} , respectively, touching L_1 on alternate vertices of Γ . In the end, we get parallel lines L_1, \dots, L_z , where $z = \frac{1}{2} \gcd(r, |t - s|)$ such that each L_i ($i = 1, \dots, z$) determines two 1-zigzagging cycles C_i^0, C_i^1 in F_{12}, F_{34} , respectively, touching L_i at alternate vertices of Γ . An example is shown in Fig. 2(c) for $r = 12, t = 5, s = 9$ with $z = 2$, where L_1 is given in black thin trace and L_2 is given in gray thin trace, (not considering here the intermittent diagonals). \square

Corollary 35. *If $\frac{1}{2} \gcd(r, |t - s|) = \gcd(r, s) = \frac{1}{2} \gcd(r, t + s) = 1$, then the 2-factors (12), (34), (13), (14) and (23) are composed by a Hamilton cycle each (a total of six Hamilton cycles), comprising the 2-factorizations (12)(34) and (14)(23).*

Proof. This is due to Remark 33 and to the quadruple equality in the statement. \square

Additional examples are provided in display (7) for fixed $t = 2$, as in Theorem 10 item 3(b). The reader is invited to do similarly for Theorem 10, items 3(a) and 3(c).

r	$s = 4$	$s = 6$	r	$s = 4$	$s = 6$	r	$s = 4$	$s = 6$
8	141		14	121	121	20	141	122
10	121		16	141	124	22	121	121
12	143	162	18	123	131	24	143	164

(7)

Corollary 36. *In all cases of Theorem 10 item 2(b), there are exactly two hamiltonian 2-factorizations. Moreover, the toroidal graphs Γ in Theorem 10 are*

1. $\Gamma(222)$, for items 1(c)–2(a);
2. $\Gamma(211)$, for item 2(b) just for $s \equiv 1 \pmod{4}$;
3. $\Gamma(112)$, for item 2(b) just for $s \equiv 3 \pmod{4}$.

Proof. The toroidal graphs in Theorem 10 items 1(c) and 2(b) behave differently from those in Theorem 34 in that the 2-factors in question are 1-zigzagging in only one of the three 2-factorizations, while the other two 1-factorizations are 2-zigzagging, namely:

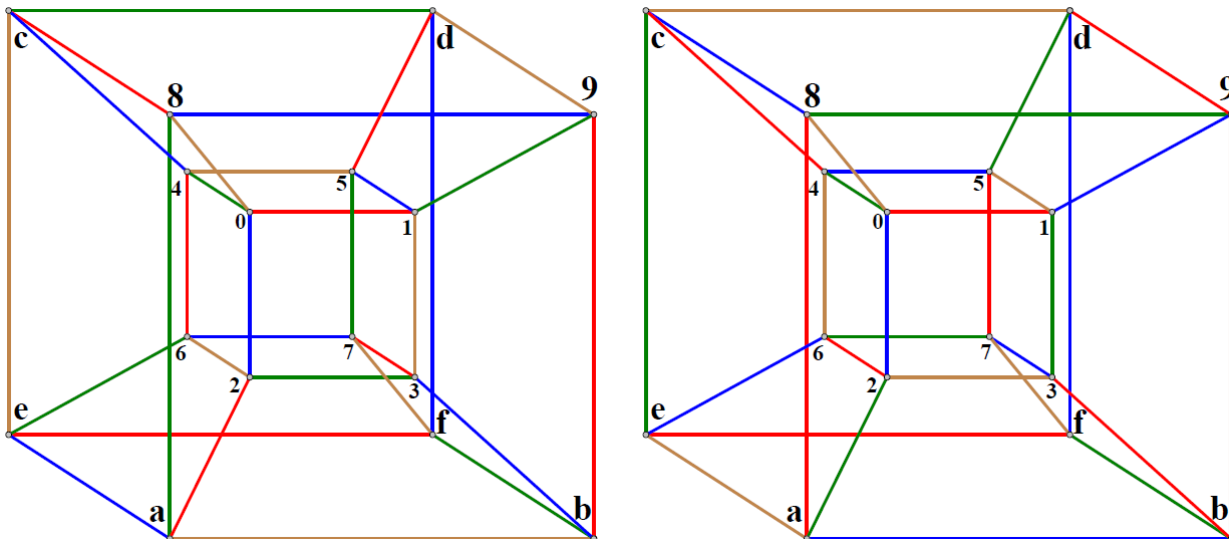


Figure 15: Two egc edge-colored 4-cube graphs.

- (a) in Theorem 10 items 1(c) and 2(b), just for $s \equiv 1 \pmod{4}$, the 1-factorization (12)(34) is 1-zigzagging and the 1-factorizations (13)(24) and (14)(23) are 2-zigzagging;
- (b) in Theorem 10 item 2(b) just for $s \equiv 3 \pmod{4}$, the 2-factorizations (12)(34)–(13)(24) are 2-zigzagging and the 2-factorization (14)(23) is 1-zigzagging.

□

8 Applications to 3-dimensional geometry

Fig. 15 redraws the two toroidal copies of Q_4 in the lower center–right of Fig. 3, (which arise respectively in Subsection 3.1 from the central–right latin squares in display (1)), as edge-colored tesseracts, in order to extract piecewise linear (PL) [20] realizations of two enantiomorphic compounds of four Möbius strips each [11, 12]. In the sequel, this results are equivalent to corresponding enantiomorphic Holden-Odom-Coxeter polylinks of four locked hollow equilateral triangles each [6, 13, 14], from a group-theoretical point of view .

8.1 Usage of the two nontrivial Latin squares in MOLs(4)

Fig. 17 contains two horizontal sets of four copies of Q_3 each. A 6-cycle ξ_i is distinguished in each such copy Q_3^i of Q_3 with a respective color i ($i = 1$ for red, $i = 2$ for blue, $i = 3$ for green and $i = 4$ for hazel). Each Q_3^i has its ξ_i with the edges marked x_i^j , where $x = t$ for a trapezoid and $x = p$ for a parallelogram (quadrangles that are the faces of PL Möbius strips as in Fig. 19), $i \in \{1, 2, 3, 4\}$ for associated color and $j \in \{h, v, d\}$ for edge direction (h for horizontal, v for vertical and d for in-depth). The top (resp. bottom) set has each Q_3^i with a one-to-one correspondence from its edges t_i^j (p_i^j) to the edges with color i and direction j in the inner (outer) copy of Q_3 in the left (resp. right) copy of Q_4 in Fig. 15.

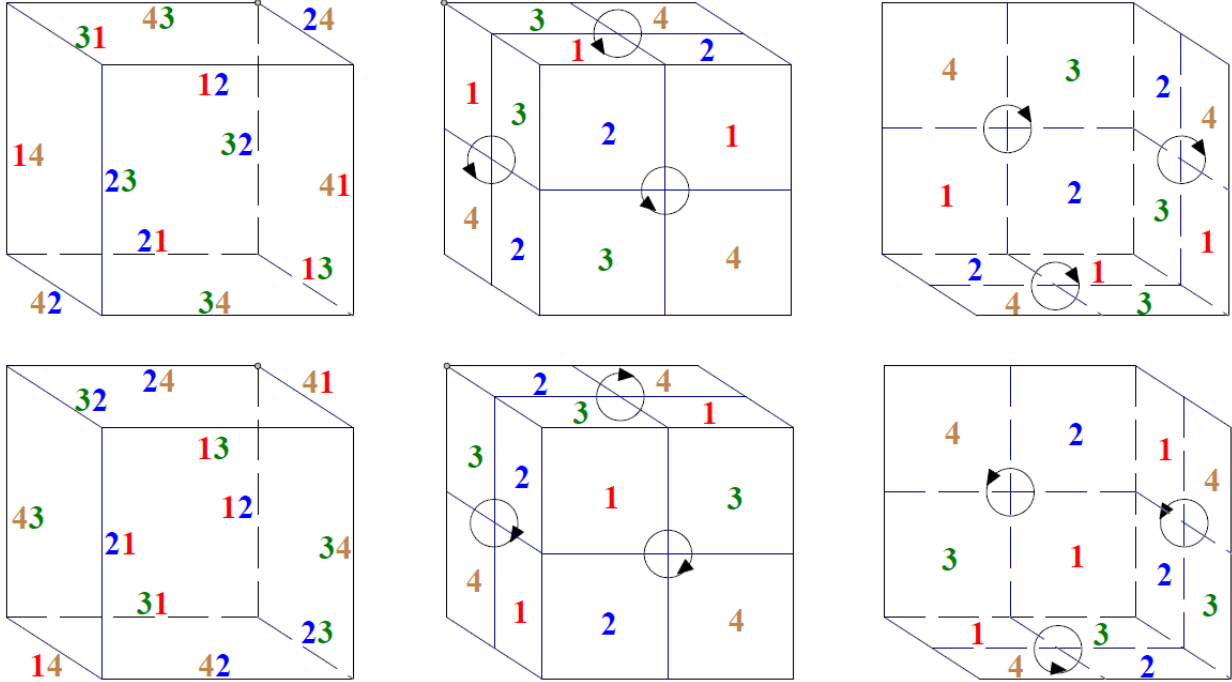


Figure 16: Assignment of pairs of colors to the edges of 3-cubes

This way, each $Q_3^i \setminus \xi_i$ in Fig. 17 is formed by two antipodal vertices that are joined by a color- i dashed axis, allowing to visualize 120° angle rotations representing color-and- $(t\text{-or-}p)$ -preserving automorphisms that will reappear in relation to Fig. 18-19.

The two leftmost 3-cubes in Fig. 16 have each of their edges assigned a pair of colors in $\{1, 2, 3, 4\}$. The first (resp. second) color is obtained from the corresponding row of 3-cubes in Fig. 17 as the color i of the only edge t_i^j (resp. p_i^j) in that edge position among the four cases in the row. This allows an assignment of a color to each face quadrant of the cube, as shown on the center and right in Fig. 16, and figuring the twenty-four such quadrants in each of the two cases. Note that the faces in these cubes are given an orientation each. The color pairs in Fig. 17 can be recovered from the quadrant colors in Fig. 16 by reading them along an edge according to the corresponding face orientation.

8.2 Compound of four PL Möbius strips

Fig. 18 depicts the union $[0, 3]^3 \subset \mathbb{R}^3$ of twenty-seven unit 3-cubes. In it, information carried by the top rows in Fig. 17 determines four PL trefoil knots, one per each color $i \in \{1, 2, 3, 4\}$. These trefoil knots are indicated in thick trace along edges of the said unit cubes. These i -colored thick-traced edges determine two parallel sides of either a trapezoid or a parallelogram, as illustrated in Fig. 19, for $i = 4 = \text{hazel color}$. In the case of a trapezoid (resp. parallelogram), the lengths of those sides are 3 internally and 1 externally (resp. 2 internally and 2 externally). The other two sides of each trapezoid or parallelogram are presented in *thin* trace in the color i to distinguish them from the *thick* trace of the trefoil knot sides. Note that the constructed trapezoids and parallelograms determine four PL

Möbius strips that give place to the following results. (Similar results for the bottom half of Fig. 17 are omitted and left for the interested reader to figure out).

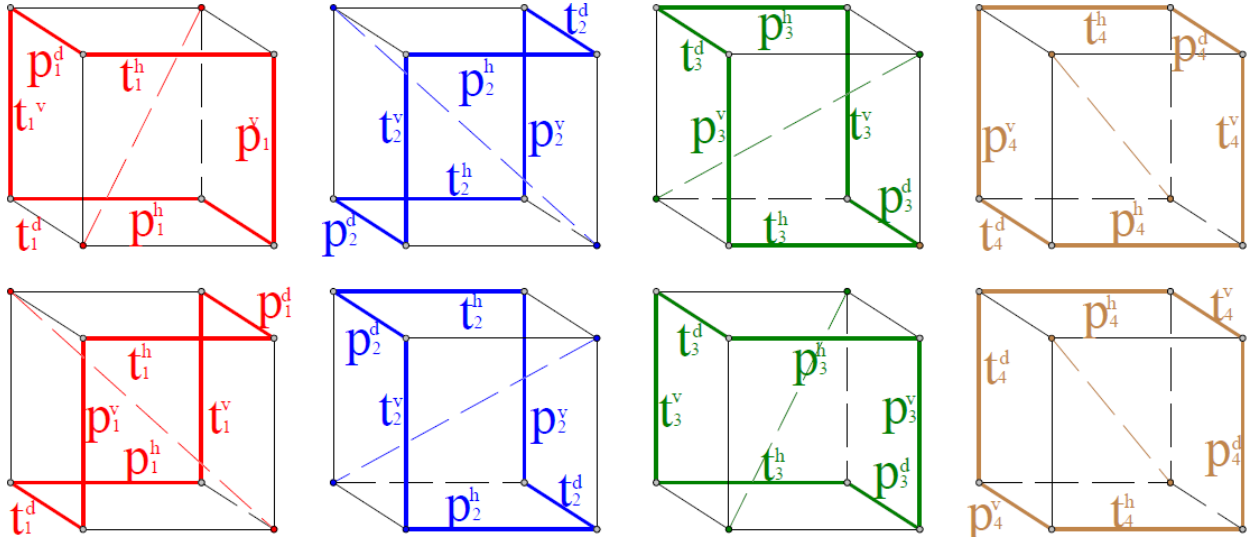


Figure 17: Edges of rotation.

Theorem 37. *There exists a maximum-area PL Möbius strip M_1 embedded in $[0, 3]^3 \setminus [1, 2]^3 \subset \mathbb{R}^3$ whose boundary is a PL closed curve C_1 formed by a minimum of segments parallel to the coordinate directions and whose end-vertices are points in \mathbb{Z}^3 .*

Proof. A strip as in the statement is represented in Fig. 19 (whose PL boundary is also present in Fig. 18 as the hazel trefoil knot), with the mentioned segments as in the following display (where, starting clockwise at the left upper corner of Fig. 19, colors of quadrilaterals are cited and, between parentheses, whether they are shown full or in part):

$gray(part)$	$green(part)$	$yellow(full)$	$gray(part)$	$green(full)$	$yellow(part)$
$[103, 203]_1^h$	$[203, 201]_2^v$	$[201, 231]_3^d$	$[231, 031]_2^h$	$[031, 032]_1^v$	$[032, 012]_2^d$
$[012, 312]_3^h$	$[312, 310]_2^v$	$[310, 320]_1^d$	$[320, 120]_2^h$	$[120, 123]_3^v$	$[123, 103]_2^d$

(8)

Here, a segment denoted $[a_1a_2a_3, b_1b_2b_3]$ stands for $[(a_1, a_2, a_3), (b_1, b_2, b_3)]$, with $a_i, b_i \in \{0, 1, 2, 3\}$, ($i = 1, 2, 3$). In (1), each of the twelve segments are appended with its length as a subindex and an element of $\{h, v, d\}$ as a superindex, where h, v , and d stand for horizontal, vertical and in-depth directions, respectively. The PL curve C_4 , a PL trefoil knot, is depicted in thick hazel trace in Fig. 18 (via unbroken unit-segment edges). \square

Theorem 38. *The maximum number of Möbius strips in $[0, 3]^3 \setminus [1, 2]^3$ as in Theorem 37 and whose boundaries have pairwise intersections of dimension 0 (i.e., isolated points) is 4.*

Proof. To prove the statement, consider Fig. 18, where C_1 is again drawn, as well as the blue PL trefoil C_2 , defined by the segments:

$$\begin{array}{cccccc}
[100, 200]_1^h & [200, 220]_2^v & [220, 223]_3^d & [223, 023]_2^h & [023, 013]_1^v & [013, 011]_2^d \\
[011, 311]_3^h & [311, 331]_2^v & [331, 332]_1^d & [332, 331]_2^h & [331, 102]_3^v & [102, 100]_2^d
\end{array} \quad (9)$$

and the green PL trefoil C_3 , defined by the segments:

$$\begin{array}{cccccc}
[133, 233]_1^h & [233, 213]_2^v & [213, 210]_3^d & [210, 010]_2^h & [010, 020]_1^v & [020, 022]_2^d \\
[022, 322]_3^h & [322, 302]_2^v & [302, 301]_1^d & [301, 101]_2^h & [101, 131]_3^v & [131, 133]_2^d
\end{array} \quad (10)$$

and the brown PL trefoil C_4 , defined by the segments:

$$\begin{array}{cccccc}
[230, 130]_1^h & [130, 110]_2^v & [110, 113]_3^d & [113, 313]_2^h & [313, 323]_1^v & [323, 321]_2^d \\
[321, 021]_3^h & [021, 001]_2^v & [001, 002]_1^d & [002, 202]_2^h & [202, 232]_3^v & [232, 230]_2^d
\end{array} \quad (11)$$

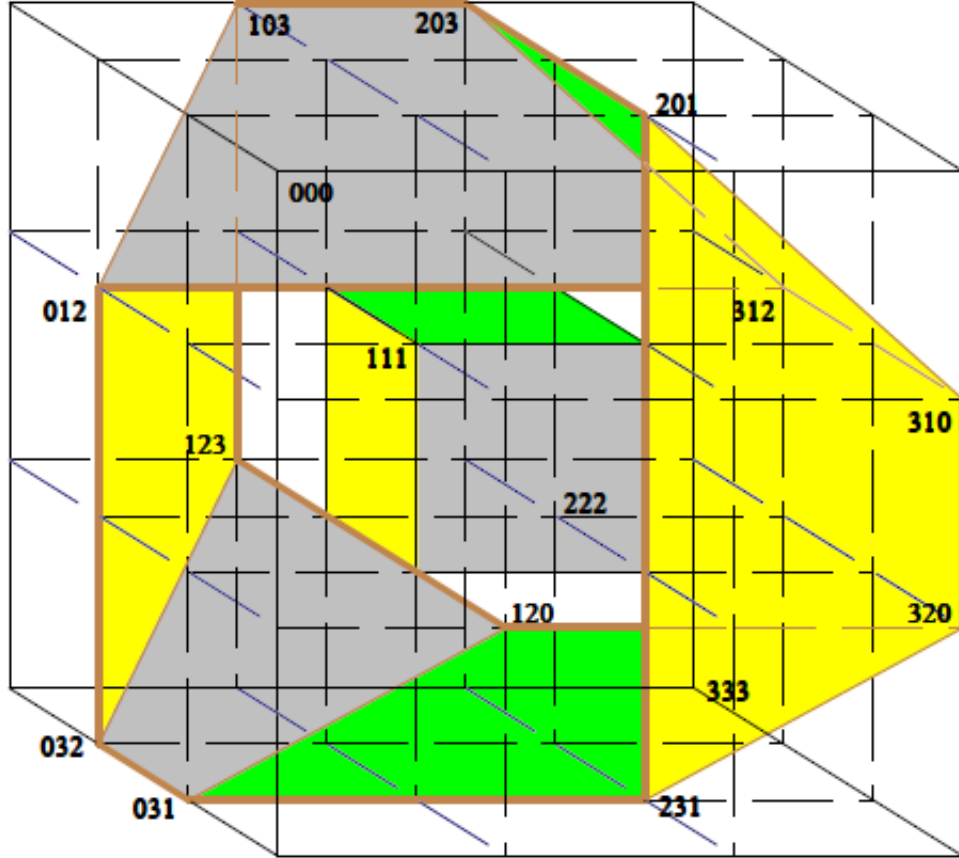


Figure 18: PL Möbius strip whose PL boundary has color 4 = hazel.

Observe that the six (maximum) planar faces of M_1 intersect C_4 in six pairs of segments, shown in display (8) vertically: first $[103, 203]_1^h$ above and $[012, 312]_3^h$ below, which form an isosceles trapezoid together with the segments $[103, 012]$ and $[203, 312]$; then, $[203, 201]_2^v$

above, and $[312, 310]_2^g$ below, which form a parallelogram together with the segments $[203, 312]$ and $[201, 310]$, etc. Similar observations can be made with respect to displays (9)–(11). We denote such planar faces in (3-6) by $t_i^h, p_i^d, t_i^v, p_i^h, t_i^d, p_i^v$, ($i \in \{1, 2, 3, 4\}$), as on the rightmost (color 4 =) hazel 3-cube in the schematic Fig. 17.

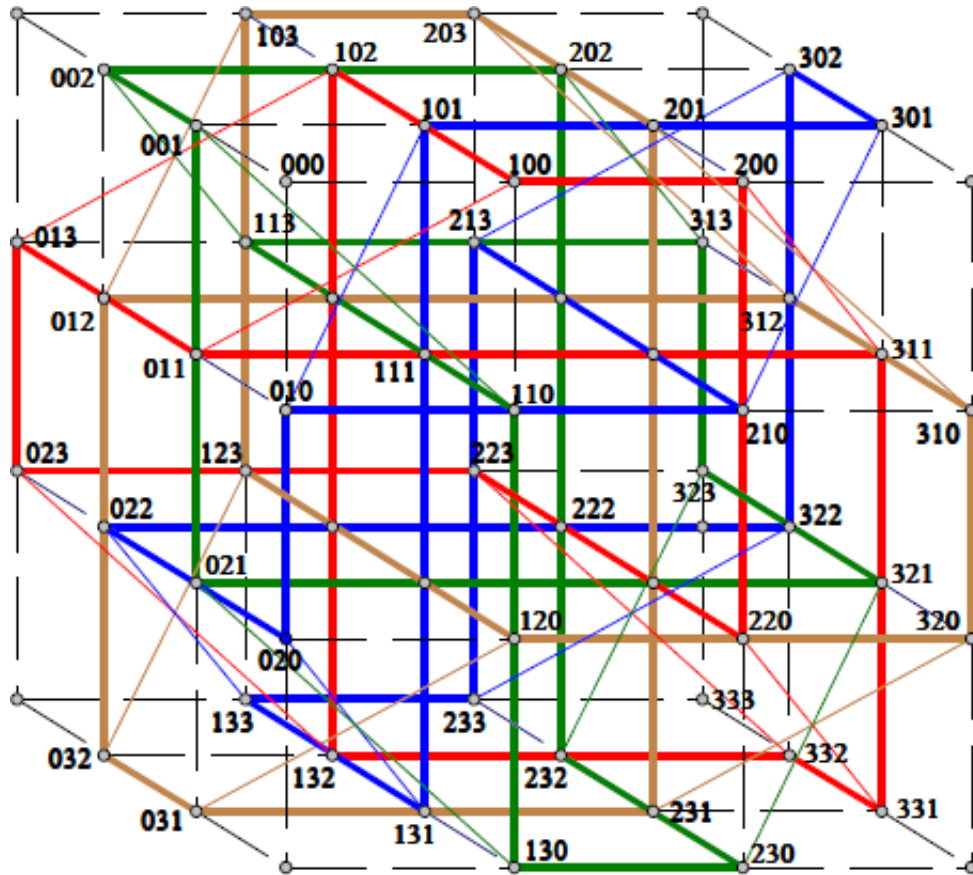


Figure 19: Four edge-disjoint PL trefoil subgraphs bounding four PL Möbius strips.

Let us denote the maximum PL Möbius strips expanded by the PL trefoil knots C_2 , C_3 and C_4 respectively as M_2 , M_3 and M_4 . Let us look at the segmental intersections of trapezoids and parallelograms in $M = M_1 \cup M_2 \cup M_3 \cup M_4$ from displays (1)–(9) above. Recall: color 1 is red, color 2 is blue, color 3 is green and color 4 is brown.

The top-front set $TF_i^h = ([000, 300] \times [000, 010] \times [000, 001]) \cap M_i$ in $[0, 3]^3$ is trapezoid t_2^h for $i = 2$ and parallelogram p_3^h for $i = 3$. In the upper leftmost cube in Fig. 16, let us call it Q , we indicate this segmental intersection by the edge-labelling pair 23, with 2 in blue and 3 in green, which are the colors used to represent C_2 and C_3 , respectively. This pair 23 labels the top-front horizontal edge in Q , corresponding to the position of $TF_2^h \cap TF_3^h$ in Fig. 18.

In all edge-labelling pairs in Q (Fig. 16), the first number is associated to a trapezoid and the second one to a parallelogram, each number printed in its associated color.

We subdivide the six faces of Q into four quarters each and label them 1 to 4, setting external counterclockwise (or internal clockwise) orientations to the faces, so that the two quarter numbers corresponding to an edge of any given face yield, via the defined orientation,

the labelling pair as defined in the previous paragraph. This is represented in the center and rightmost cubes in Fig. 16.

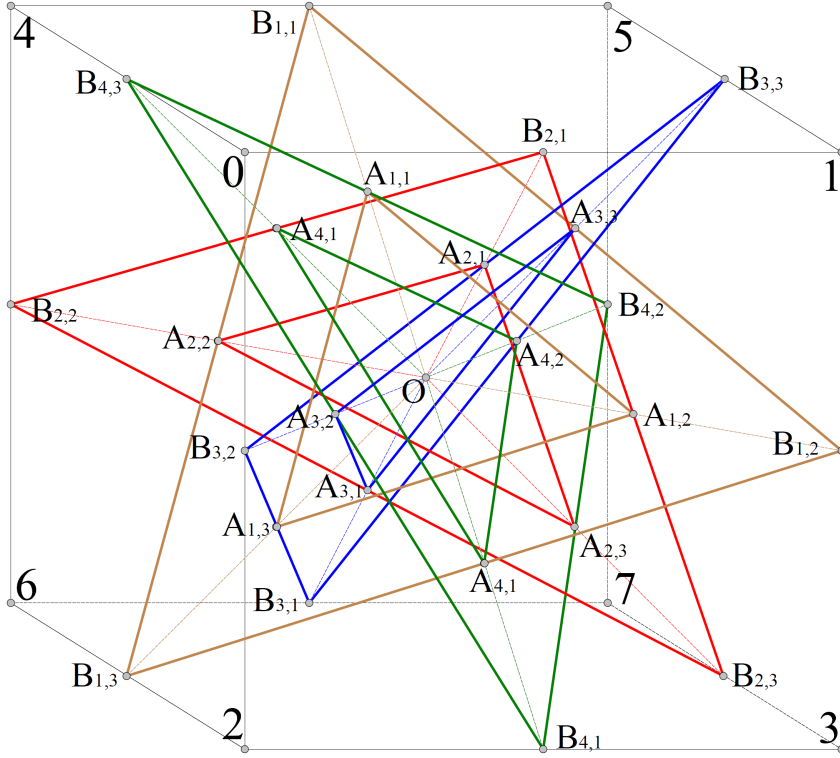


Figure 20: Odom-Coxeter polylink.

We can identify the cube Q with the union of the pairwise distinct intersections $M_i \cap M_j$, ($1 \leq i < j \leq 4$). This way, Q becomes formed by the segments:

$$\begin{aligned}
& [(0.5,0.5,0.5),(2.5,0.5,0.5)]_2^3, [(0.5,2.5,0.5),(2.5,2.5,0.5)]_1^4, [(0.5,0.5,2.5),(2.5,0.5,2.5)]_3^2, [(0.5,2.5,2.5),(2.5,2.5,2.5)]_4^1, \\
& [(0.5,0.5,0.5),(0.5,2.5,0.5)]_3^4, [(2.5,0.5,0.5),(2.5,2.5,0.5)]_2^1, [(0.5,0.5,2.5),(0.5,2.5,2.5)]_4^3, [(2.5,0.5,2.5),(2.5,2.5,2.5)]_2^1, \\
& [(0.5,0.5,0.5),(0.5,0.5,2.5)]_4^2, [(2.5,0.5,0.5),(2.5,0.5,2.5)]_1^3, [(0.5,2.5,0.5),(0.5,2.5,2.5)]_2^4, [(2.5,2.5,0.5),(2.5,2.5,2.5)]_3^1,
\end{aligned} \tag{12}$$

where each segment is suffixed with its trapezoid color number as a subindex and its parallelogram color number as a superindex. The first to third lines in (10) display those segments of Q parallel to the first to third coordinates, respectively. Fig. 17 represents the Möbius strips M_i in Q , for $i = 1, 2, 3, 4$, with the i -colored edges corresponding to the trapezoids and parallelograms of each M_i labeled via x_i^j , ($x = t$ for trapezoid; $x = p$ for parallelogram; $j \in \{h, v, d\}$ for horizontal, vertical and in-depth edges of Q , respectively). \square

Theorem 39. *The automorphism group $G = \text{Aut}(\bigcup_{i=1}^4 M_i)$ of $\bigcup_{i=1}^4 M_i$ is isomorphic to $\mathbb{Z}_2 \times \mathbb{Z}_2 \times \mathbb{Z}_2$. Moreover, there are only two 4-PL-Möbius-strip compounds, one of which (M_4) is the one with PL Möbius strip boundaries depicted as the PL trefoils in Fig. 18. Furthermore, these two compounds are enantiomorphic.*

Proof. By way of the reflection F_O of $[0, 3]^3 \setminus [1, 2]^3$ about the central vertex $O = (1.5, 1.5, 1.5)$ of $[0, 3]^3$, each M_i is transformed bijectively and homeomorphically into M_{5-i} , for $i = 1, 2, 3, 4$. The 180° angle rotations R_d^2, R_v^2, R_h^2 of $[0, 3]^3$ about the in-depth axis $x_1 = x_2 = 1.5$, the vertical axis $x_1 = x_3 = 1.5$ and the horizontal axis $x_2 = x_3 = 1.5$, respectively, form the following respective transpositions on the vertices of $[0, 3]^3$:

$$\begin{aligned} & ((x_1, x_2, x_3), (3 - x_1, 3 - x_2, x_3)), \forall x_i \in \{0, 3\}, (i = 1, 2, 3) \\ & ((x_1, x_2, x_3), (3 - x_1, x_2, 3 - x_3)), \forall x_i \in \{0, 3\}, (i = 1, 2, 3) \text{ and} \\ & ((x_1, x_2, x_3), (x_1, 3 - x_2, 3 - x_3)), \forall x_i \in \{0, 3\}, (i = 1, 2, 3) \end{aligned} \quad (13)$$

and determine the following permutations of Möbius strips M_i , ($i = 1, 2, 3, 4$):

$$(M_1, M_3)(M_2, M_4), (M_1, M_2)(M_3, M_4) \text{ and } (M_1, M_4)(M_2, M_3). \quad (14)$$

On the other hand, neither the reflections on the coordinate planes at $O = (1.5, 1.5, 1.5)$ nor the $\pm 90^\circ$ angle rotations $R_d, R_d^3, R_v, R_v^3, R_h, R_h^3$ preserve the union $\bigcup_{i=1}^4 M_i$ but yield a 4-PL-Möbius-strip compound that is enantiomorphic to $\bigcup_{i=1}^4 M_i$. Moreover, G is generated by F_O, R_d, R_v and R_h . \square

8.3 Polylink of four hollow triangles

A sculpture by G. P. Odom Jr., see Fig. 20, was analyzed by H. S. M. Coxeter [6], for its geometric and symmetric properties. According to [21, p. 270], Odom and Coxeter were unaware of the earlier discovery [13] of this by A. Holden, who called it a *regular polylink of four locked hollow triangles* [14].

We relate the top Möbius-strip compound above to this structure, noting that the centers of the maximum linear parts of the PL trefoil knots C_i ($i = 1, 2, 3, 4$) are the vertices of four corresponding equilateral triangles, namely (in the order of the triangle colors):

$$\begin{array}{l} 1 : (1.5, 0, 3), (3, 1.5, 0), (0, 3, 1.5); \\ 3 : (1.5, 3, 3), (0, 1.5, 0), (3, 0, 1.5); \end{array} \left| \begin{array}{l} 2 : (1.5, 0, 0), (0, 1.5, 3), (3, 3, 1.5); \\ 4 : (1.5, 3, 0), (3, 1.5, 3), (0, 0, 1.5). \end{array} \right. \quad (15)$$

Each of these triangles T_i ($i = 1, 2, 3, 4$), gives place to a hollow triangle (i.e., a planar region bounded by two homothetic and concentric equilateral triangles [6]) by removing from T_i the equilateral triangle T'_i whose vertices are the midpoints of the segments between the vertices of T_i (display (15)) and $O = (1.5, 1.5, 1.5)$. Characterized by colors, these midpoints are

$$\begin{aligned} 1 : & (1.50, 0.75, 2.25), (2, 25, 1.50, 0.75), (0.75, 2.25, 1.50); \\ 2 : & (1.50, 0.75, 0.75), (0.75, 1.50, 2.25), (2.25, 2.25, 1.50); \\ 3 : & (1.50, 2.25, 2.25), (0.75, 1.50, 0.75), (2.25, 0.75, 1.50); \\ 4 : & (1.50, 2.25, 0.75), (2.25, 1.50, 2.25), (0.75, 0.75, 1.50). \end{aligned} \quad (16)$$

The centers in display (15) are the vertices of an Archimedean cuboctahedron. Consider the midpoints of the sides of the triangles T_i , namely:

$$\begin{aligned}
1 : & (2.25, 0.75, 1.50), (1.50, 2.25, 0.75), (0.75, 1.50, 2.25); \\
2 : & (0.75, 0.75, 1.50), (1.50, 2.25, 2.25), (2.25, 1.50, 0.75); \\
3 : & (0.75, 2.25, 1.50), (1.50, 0.75, 0.75), (2.25, 1.50, 2.25); \\
4 : & (2.25, 2.25, 1.50), (1.50, 0.75, 2.25); (0.75, 1.50, 0.75).
\end{aligned} \tag{17}$$

By expressing the 3-tuples in (16) via a 4×3 -matrix $\{A_{i,j}; i = 1, 2, 3; j = 1, 2, 3, 4\}$, we have the following correspondence from (16) to (17), in terms of the notation in Fig. 20:

$$\begin{pmatrix} A_{1,1} & A_{1,2} & A_{1,3} \\ A_{2,1} & A_{2,2} & A_{2,3} \\ A_{3,1} & A_{3,2} & A_{3,3} \\ A_{4,1} & A_{4,2} & A_{4,3} \end{pmatrix} \rightarrow \begin{pmatrix} B_{1,12} & B_{1,23} & B_{1,31} \\ B_{2,12} & B_{2,23} & B_{2,31} \\ B_{3,12} & B_{3,23} & B_{3,31} \\ B_{4,12} & B_{4,23} & B_{4,31} \end{pmatrix} = \begin{pmatrix} A_{3,3} & A_{4,1} & A_{2,2} \\ A_{4,3} & A_{3,1} & A_{1,2} \\ A_{1,3} & A_{2,1} & A_{4,2} \\ A_{2,3} & A_{1,1} & A_{3,2} \end{pmatrix} \tag{18}$$

meaning each midpoint $B_{i,jk}$ of a T_i between $B_{i,j}$ and $B_{i,k}$ equals a vertex $A_{i',j'}$ of some $T_{i'}$, and vice-versa, as in Fig. 20. Take each T_i as the 6-cycle of its vertices and side midpoints:

$$\begin{aligned}
T_1 &= (B_{1,1} \ A_{3,3} \ B_{1,2} \ A_{4,1} \ B_{1,3} \ A_{2,2}); \\
T_2 &= (B_{2,1} \ A_{1,2} \ B_{2,3} \ A_{3,1} \ B_{2,2} \ A_{4,1}); \\
T_3 &= (B_{3,1} \ A_{1,3} \ B_{3,2} \ A_{2,1} \ B_{3,3} \ A_{4,2}); \\
T_4 &= (B_{4,1} \ A_{1,1} \ B_{4,2} \ A_{2,3} \ B_{4,1} \ A_{3,2}).
\end{aligned} \tag{19}$$

Corollary 40. *The automorphism group of the union $\bigcup_{i=1}^4 T_i$ is $G = \text{Aut}(\bigcup_{i=1}^4 M_i) = \text{Aut}(\bigcup_{i=1}^4 T_i)$. In addition, $G_i = \text{Aut}(M_i) = \text{Aut}(T_i)$, for each $i = 1, 2, 3, 4$, is isomorphic to the dihedral group of six elements. Moreover, there are only two polylinks of four hollow triangles in $[0, 3]^3$, including $\bigcup_{i=1}^4 T_i$, and these two polylinks are enantiomorphic.*

Proof. By expressing, as in Fig. 20, the vertices of $[0, 3]^3$ by:

$$\mathbf{0} = 000, \quad \mathbf{1} = 300, \quad \mathbf{2} = 030, \quad \mathbf{3} = 330, \quad \mathbf{4} = 003, \quad \mathbf{5} = 303, \quad \mathbf{6} = 033, \quad \mathbf{7} = 033, \tag{20}$$

we notice that the $\pm 120^\circ$ angle rotations of $[0, 3]^3$ around the axis line determined by the two points of color i in Q , as indicated in Fig. 17, correspond respectively to the permutations:

$$\begin{aligned}
\text{Color 1 : } R_1 &= (\mathbf{124})(\mathbf{365}) \quad \text{and} \quad R_1^{-1} = (\mathbf{142})(\mathbf{563}); \\
\text{Color 2 : } R_2 &= (\mathbf{036})(\mathbf{174}) \quad \text{and} \quad R_2^{-1} = (\mathbf{063})(\mathbf{147}); \\
\text{Color 3 : } R_3 &= (\mathbf{065})(\mathbf{271}) \quad \text{and} \quad R_3^{-1} = (\mathbf{056})(\mathbf{217}); \\
\text{Color 4 : } R_4 &= (\mathbf{247})(\mathbf{053}) \quad \text{and} \quad R_4^{-1} = (\mathbf{274})(\mathbf{035}),
\end{aligned} \tag{21}$$

where color 1 is red, color 2 is blue, color 3 is green and color 4 is hazel; notice also that the axes in Q corresponding to these colors are:

$$\begin{aligned}
& [(0.5, 0.5, 0.5), (2.5, 2.5, 2.5)], \quad [(0.5, 2.5, 0.5), (2.5, 0.5, 2.5)], \\
& [(0.5, 0.5, 2.5), (2.5, 2.5, 0.5)], \quad [(2.5, 0.5, 0.5), (0.5, 2.5, 2.5)].
\end{aligned}$$

The rest of the statement arises from Theorem 39. The fact that there are two polylinks of four hollow triangles in $[0, 3]^3$ that are enantiomorphic is inherited from Theorem 39. \square

References

- [1] C. Armanios, *A new 5-valent distance transitive graph*, Ars Combin. **19A** (1985), 77–85.
- [2] A. Brouwer, A. Neumaier, A. Cohen, *Distance-Regular Graphs*, Springer-Verlag, 1998.
- [3] C. J. Colbourn, J. H. Dinitz, *Handbook of Combinatorial Designs* (2nd ed.), Boca Raton: Chapman & Hall/ CRC, (2007).
- [4] J. H. Conway, N. J. A. Sloane, *Sphere Packings, Lattices and Groups*, (3rd ed.), Berlin, New York: Springer-Verlag, (1999).
- [5] S. L. R. Costa, R. Muniz, E. Agustini, R. Palazzo, *Graphs, Tessellations and Perfect Codes in Flat Tori*, IEEE Transactions on Information Theory, **50-10**(2004), 2363-2377.
- [6] H. S. M. Coxeter, *Symmetrical Combinations of Three or Four Hollow Triangles*, The Mathematical Intelligencer, **16**(3) (1994), 25–30.
- [7] H. S. M. Coxeter, *Self-Dual Configurations and Regular Graphs*, Bull. Amer. Math. Soc. **56** (1950), 413–455.
- [8] P. R. Cromwell, *Polyhedra*, Cambridge Univ. Press, Cambridge UK (1997).
- [9] I. J. Dejter, O. Serra, *Efficient dominating sets in Cayley graphs*, Discrete Applied Mathematics **129**(2–3) (2002), 319–328.
- [10] E. Eiben, R. Jajcay, P. Šparl, *Symmetry properties of generalized graph truncations*, J. Combin. Theory, Ser. B **137** (2019) 29–131.
- [11] D. Fuchs, S. Tabachnikov, *Mathematical Omnibus: Thirty Lectures on Classic Mathematics*, 2007, 199–206, at <http://www.math.psu.edu/tabachni/Books/tabachni.pdf>
- [12] D. Hilbert, S. Cohn-Vossen, *Geometry and the Imagination* (2nd ed.), Chelsea, 1952.
- [13] A. Holden, *Shapes, Spaces and Symmetry*, Columbia Univ. Press, 1971.
- [14] A. Holden, *Regular Polylinks*, Structural Topology, **4** (1980), 41–45.
- [15] W. Imrich, S. Klavžar, D. F. Rall, *Graphs and their cartesian products*, A. K. Peters, (2008).
- [16] P. Potočník, P. Spiga, G. Verret, *A census of cubic vertex-transitive graphs*
<https://staff.matapp.unimib.it/~spiga/census.html>.
- [17] P. Potočník, J. Vidali, *Girth-regular graphs*, Ars Mathematica Contemporanea, **17** (2019), 349–368.
- [18] P. Potočník, S. Wilson, *Tetravalent edge-transitive graphs of girth at most 4*, Jour. Combin. Theory, ser. B, **97** (2007), 217–236.

- [19] P. Potočnik, S. Wilson, *Linking-ring structures and tetravalent semisymmetric graphs*, Ars. Math. Contemporanea, **7** (2014), 341–352.
- [20] C. P. Rourke, B. J. Sanderson, *Introduction to Piecewise-Linear Topology*, Springer, New York, NY, 1972.
- [21] D. Schattschneider *Coxeter and the Artists: 2-Way Inspiration*, in *The Coxeter Legacy, Reflections and Projections*, (ed. C. Davis et al.), Amer. Math. Soc., 2006.
- [22] W. D. Wallis, *One-Factorizations (Math. and its Appl.)*, Springer, NY, 1997.
- [23] S. Wilson, *Uniform maps on the Klein bottle*, Jour. for Geom. and Graphics, **10**(2) (2006), 161–171.
- [24] S. Wilson, P. Potočnik, *Recipes for edge-transitive tetravalent graphs*, arXiv:1608.04158.